ERDC TR-07-12

US Army Corps of Engineers®
Engineer Research and Development Center

*National Shoreline Erosion Control Development and Demonstration Program*

# Flow Model Study for Section 227 Demonstration Project in Allegan County, Michigan

Clarissa P. Hansen, Stacy E. Howington, and M. Eileen Glynn

September 2007

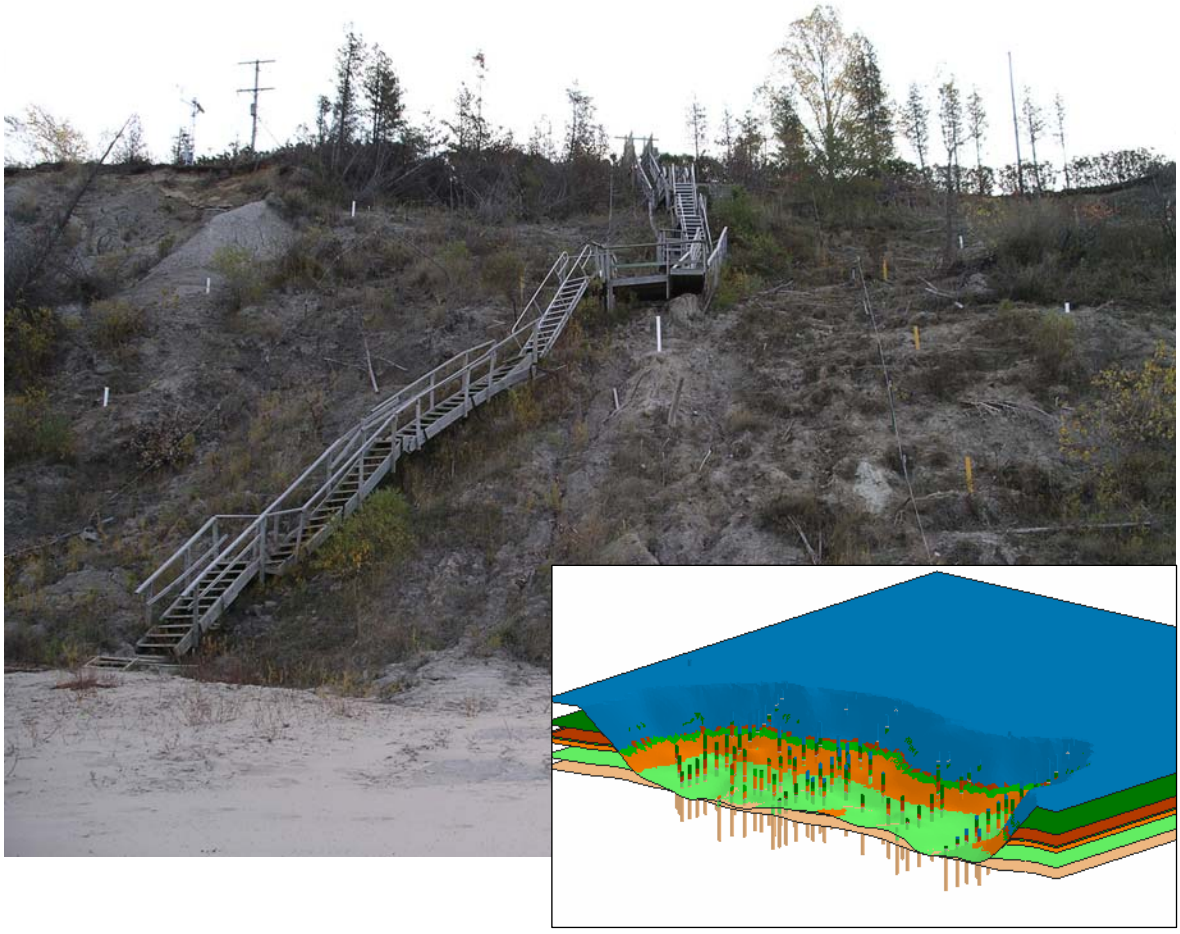

Engineer Research and Development Center

National Shoreline Erosion Control
Development and Demonstration Program

ERDC TR-07-12
September 2007

# Flow Model Study for Section 227 Demonstration Project in Allegan County, Michigan

Clarissa P. Hansen

*Malcolm Pirnie, Inc.*
*640 Freedom Business Center*
*King of Prussia, PA 19406*

Stacy E. Howington

*Coastal and Hydraulics Laboratory*
*U.S. Army Engineer Research and Development Center*
*3909 Halls Ferry Road*
*Vicksburg, MS 39180-6199*

M. Eileen Glynn

*Geotechnical and Structures Laboratory*
*U.S. Army Engineer Research and Development Center*
*3909 Halls Ferry Road*
*Vicksburg, MS 39180-6199*

Final report



Prepared for U.S. Army Corps of Engineers
Washington, DC 20314-1000

**Abstract:** The National Shoreline Erosion Control Development and Demonstration Program (Section 227) is authorized by Congress under Section 227 of the Water Resources and Development Act of 1996. The program provided funding to research projects for the development and evaluation of innovative methods of shoreline erosion abatement. This report describes a numerical flow model developed for the Allegan County Bluff Stabilization Project within the Section 227 Demonstration Program. The Bluff Stabilization Site is located just north of Southaven, MI, and lies on the east coast of Lake Michigan.

Bluff recession and subsequent property loss from bluff erosion is a perpetual process along the coastlines of the Great Lakes. Historically, engineers have protected the toe of the bluff from erosion with seawalls, revetments, dikes, etc., to slow bluff recession. For many bluffs, toe protection helps little because the bluff (slope) frequently fails above the protected toe, at elevations affected by perched water tables exiting at the bluff face.

The Bluff Stabilization Project has focused on the study and control of the groundwater within the bluffs and measurement of its effect on slope stability. The project has spanned over 11 years, led by Dr. Ronald Chase at Western Michigan University, Kalamazoo, MI. The many years of data exhibit a positive correlation between slope movement, freezing ambient air temperatures, and increased soil pore pressures. Thus, decreasing the pore pressures during freezing temperatures may reduce bluff recession.

A dewatering program was started in 2005 to test this hypothesis. This report describes the development of a numerical model of groundwater flow for the purpose of optimizing pumping at the test site. The flow model was constructed using the Groundwater Modeling System (GMS) with the computational code, ADaptive Hydrology/Hydraulics (ADH).

# Contents

# Figures and Tables

## Figures

## Tables

# Preface

This study was funded by The National Shoreline Erosion Control Development and Demonstration Program (Section 227) of the Water Resources and Development Act of 1996. This work was guided by the Section 227 Program Manager William R. Curtis, Technical Programs Office (TPO), Coastal and Hydraulics Laboratory (CHL), U.S. Army Engineer Research and Development Center (ERDC), and Technical Director Jack Davis, TPO. The work was completed by Clarissa P. Hansen, Malcolm Pirnie, Inc., formerly of CHL, and Dr. Stacy E. Howington, Hydraulics Systems Branch (HSB), Flood and Storm Protection Division (FSPD), CHL. The work was supervised by Earl V. Edris, Chief, HSB, and Bruce A. Ebersole, Chief, FSPD.

M. Eileen Glynn, Geotechnical and Earthquake Engineering Branch (GEEB), Geosciences and Structures Division (GSD), Geotechnical and Structures Laboratory (GSL), ERDC, was the Principal Investigator for the Allegan Bluff Stabilization Project. She contributed to the content of this report, under the general supervision of Dr. Joseph P. Koester, Chief, GEEB; and Dr. Robert L. Hall, Chief, GSD.

Thomas W. Richardson and Dr. David W. Pittman were the directors of CHL and GSL, respectively. Dr. William D. Martin and Dr. William P. Grogan were the Deputy Directors of CHL and GSL, respectively.

COL Richard B. Jenkins was Commander and Executive Director of ERDC. Dr. James R. Houston was Director.

# Unit Conversion Factors

| Multiply | By | To Obtain |
|---|---|---|
| acres | 4,046.873 | square meters |
| cubic feet | 0.02831685 | cubic meters |
| feet | 0.3048 | meters |
| gallons (U.S. liquid) | 3.785412 E-03 | cubic meters |
| inches | 0.0254 | meters |
| miles (U.S. statute) | 1,609.347 | meters |
| yards | 0.9144 | meters |

# 1 Introduction

The National Shoreline Erosion Control Development and Demonstration Program is authorized by Congress under Section 227 of the Water Resources and Development Act of 1996. The program provides funding to several research projects for the development and evaluation of innovative methods of shoreline erosion abatement. Demonstration projects were selected throughout the United States along the Atlantic Ocean, Pacific Ocean, Gulf of Mexico, and the Great Lakes. The Allegan County, MI, demonstration site is just north of South Haven, MI, on the eastern shore of Lake Michigan where the bluffs are made up of heterogeneous glacial soils.

Normally, bluff recession is attributed to toe erosion from storm waves. Although the effects of groundwater are known to contribute to instability, they are often considered to be a secondary cause of failure, and mitigation strategies seldom address the groundwater component.

For over 10 years, a study team led by Dr. Ronald Chase of Western Michigan University has extensively monitored a 16-km reach of the Lake Michigan bluffs. The results of their study seem to point to groundwater fluctuations as a major cause of bluff failures (Chase et al. 2001b). Most catastrophic failure events have occurred during bluff face freezing or after the rise of groundwater levels. The wave scouring that typically occurs at the toe is often removing material that had already been displaced from above.

Much of the funding for this demonstration project has gone to the installation and maintenance of monitoring equipment and extraction wells at three sites along the shore of Lake Michigan. The purpose of these construction wells was to dewater the bluff faces during the fall and winter and prevent annual spring slope failures.

In addition, some of the funding was applied to the construction of a numerical flow model of one of the three sites. This model would attempt to reproduce the groundwater conditions before and after dewatering. Future plans for the numerical model include coupling it with a large deformation model and a heat transport model to more accurately model the slope failure mechanisms. This report describes the groundwater flow model.

# 2 Overview of Miami Park South Site

The site selected for application of a flow model was the Miami Park South site, the southernmost site of the three being evaluated as part of this demonstration project. The geology at this site consists of alternating layers of clay and sand, all overlain by a layer of clay-rich diamicton till. The layering of the materials results in three distinct water tables, the lowest of which is hydraulically connected to Lake Michigan. The upper two water tables release water at several seep points on the bluff face.

The bluff has moved significantly over the last 10 years of observation. A pole and cable system designed and installed by Dr. Chase allowed his team to keep track of the bluff movement and create a cross-sectional drawing along each of the cable lines showing the current material distribution beneath the surface (Chase et al. 2001a). These drawings, along with a rotosonic borehole behind the bluff face, were invaluable in setting up the material distribution for the computational model. In the fall of 2003, when drilling for the dewatering wells and piezometers took place, the data from the drilling was shown to closely match the cross-sectional information previously estimated.

Dewatering wells were installed along with piezometers and inclinometers in the northern two-thirds of the Miami Park South site. The southern third of the site is the control section. Although a few piezometers and inclinometers were installed to monitor the site, no dewatering wells were installed.

# 3 Selection of a Modeling Code

The modeling code applied to this project was selected based on the hydrogeologic conditions at the site. The existence of multiple water tables precluded the use of some common flow models that ignore the unsaturated zone or that assume a single water table. Because the geology near the bluff face is so complex due to multiple historic failures, a model running on an unstructured mesh was selected to allow a more accurate simulation of the material distribution.

The model selected was ADaptive Hydrology/Hydraulics (ADH) (Schmidt 1995; Howington et al. 1999). Early development on ADH began in 1995 led by Joe Schmidt, an engineer with the Hydraulics Laboratory, at the U.S. Army Engineer Waterways Experiment Station (WES). It began as a groundwater model based on some earlier work in the area of mesh adaption. Continued expansion of the ADH code has resulted in the addition of other hydrologic equations since that time. Today, a large team of engineers at the U.S. Army Engineer Research and Development Center (ERDC) continues to develop the model code.

ADH was built as a centralized computational engine, encompassing finite element utilities, preconditioners, solvers, and input/output subroutines. This computational engine can then be linked to one or more equation sets. In addition to saturated and unsaturated groundwater flow equation, ADH currently includes the shallow-water equations and the Navier-Stokes equations. ADH has been developed so that it is simple to add other equations to the toolbox and solve them using the fundamental set of utilities.

The solutions to the governing equations in ADH are calculated using the finite element method applied to unstructured computational meshes. Three-dimensional (3-D) meshes are composed of tetrahedral (four node) elements, while two-dimensional (2-D) meshes are made up of triangular elements. Separate equations can be coupled to allow multi-physics modeling, such as groundwater-surface water interaction modeling. ADH also uses message passing to run in parallel, allowing large models to be run more quickly through the use of a multiprocessor supercomputer or cluster. Finally, ADH includes options to adapt the mesh or automatically add or remove refinement from the user-defined mesh. Extra refinement is often necessary in areas where there is a steep gradient in the solution

variable. Where the gradient is mostly flat or constant, this refinement can be loosened to reduce computational time. ADH can adapt the mesh with each time-step, a useful capability in cases where the location of the high gradient is moving, as with a contaminant transport model of a moving plume.

The interface used to set up the model and view the results is the Department of Defense Groundwater Modeling System (GMS). First released in 1994, GMS includes interfaces to several common groundwater models. It also incorporates advanced 3-D post-processing tools for viewing model results.

# 4 Model Overview

The ADH model built for the Miami Park South site is roughly rectangular in shape. The western boundary coincides with the toe of the bluff. The eastern boundary is about 450 ft inland from that location. This distance was selected because it was far away from three standpipes located near the middle of the model domain. Several slug tests were run in these standpipes for transient calibration purposes, and the model boundary must be well outside the zone of influence of these wells. The north and south boundaries were placed outside the area of the bluff face monitoring piezometers and dewatering wells. The total area of the model domain is just less than 5 acres.

The process used to build the model involves:

1. Setting the geologic material distribution based on borehole data and known failure history
2. Building a computational mesh of the area with element material properties being set according to the knowledge of the geology
3. Assigning the boundary conditions and source/sink terms to the mesh nodes and elements
4. Calibrating
    - Steady-state calibration: The model is set up with no sources or sinks and all boundary conditions are set constant. Material properties and boundary condition values are slowly altered until the static heads at the locations of the three standpipes match those calculated by the model.
    - Transient flux calibration: The hydraulic conductivity values are further calibrated by reproducing the fluxes measured during the pumping period of some modified slug tests performed in May 2004.
    - Transient storage calibration: The storage values are calibrated by matching the heads measured during the recovery period at the end of the modified slug tests.
5. Making two final runs with the dewatering wells on. First a 2-hr run is made to compare the piezometer responses to those measured in the field. When there is more confidence in the model's ability to reproduce field conditions, the bluff wells can be turned on during a longer model run to allow an analysis of the effectiveness of the dewatering scheme.

# 5 Creating Computational Mesh

One of the most challenging parts of the model has been the creation of a computational mesh. The geology is highly complicated in the area of the bluff face and different from the sort of material distribution normally used in groundwater studies. Few groundwater studies attempt to model heterogeneity in a failure zone as we have done. Many computational meshes for groundwater models fit into the category of a “birthday cake” model, with continuous layers representing different materials. The 3-D meshing algorithm available in GMS results in a layered mesh. Although the back section of the Miami Park South mesh is clearly layered, the disturbed sections at the bluff face make this meshing technique difficult to use.

The geology became more complicated after some observation of the locations of the most productive wells during a May 2004 site visit. Measurement of the head in the upper diamicton layer in the standpipe located 75 ft behind the bluff showed that the upper water table was within a couple of feet of the ground surface. Despite the high water table, all of the upper tier wells on the bluff face were dry and unable to pump any water. In addition, many of the middle tier wells were dry. This condition led to the belief that the fault line caused by previous slope failures was hydraulically important as it was separating the bluff system from the system located less than 100 ft inland. In order to match these flow features, the fault line needed to be included in the model. This was accomplished by interpolating the location of the deepest fault where movement had caused a smear zone as the clay layers slid past other layers. This resulted in a bowl-shaped surface, which was expanded to a 4-ft-thick zone of clay-like material, termed “smear”.

The bluff face had been carefully surveyed by a team led by Dr. Chase. The resulting contour map was instrumental in creating a TIN (triangulated irregular network) of the ground surface (Figure 1).

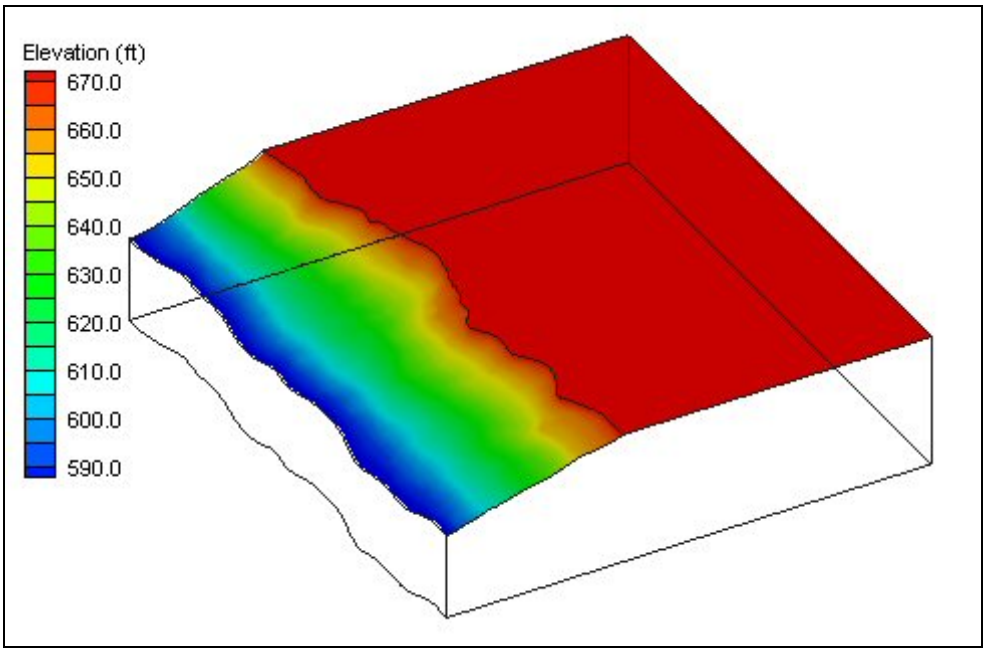


Figure 1. TIN describing ground surface.

The task of building a 3-D mesh matching the complicated geology, the smear zone and the layered system behind the bluff proved challenging. Although early creative attempts were fairly successful, the creation of the final mesh was made possible by the improvements made to the horizons method in GMS v6.0 released in 2005.

## Horizons method

The horizons method is based on the idea that the deepest layers in a subsurface system were deposited before the upper layers. The contacts between separate material types in a borehole are numbered by the order in which those materials were laid down. The horizon numbers refer to the tops of each of the layers. The user must also designate a "primary TIN" which defines the extents of the resulting solids and the resolution of the vertices on the top and bottom of each solid. More refined primary TINs result in smoother solids, but require more time to build.

When the user selects the command to convert the horizons to solids, GMS starts with the smallest horizon number, and interpolates a surface to the primary TIN. This becomes the top of the lowest layer. The process continues upward as the tops of each layer are interpolated in succession. In each case, if the top of a lower layer is interpolated to a point higher than that of an upper layer, the upper layer is cut off and the lower layer is allowed to poke through. The end result of the process is a set of solids

defining the model area (Lemon 2003a, 2003b). A simple example of a set of boreholes with horizons is shown in Figure 2 and Figure 3.

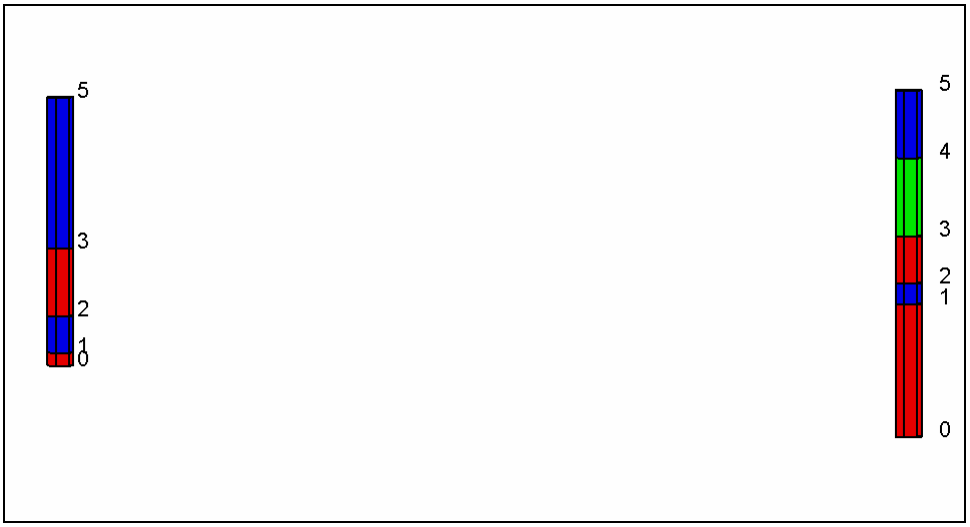


Figure 2. Two sample boreholes with horizon IDs assigned.

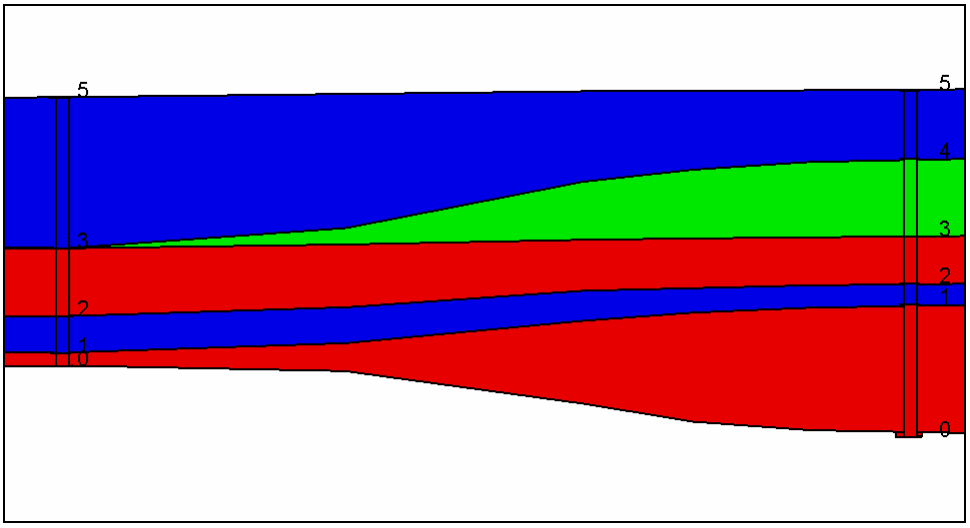


Figure 3. Two sample boreholes with horizons assigned and cross section of resulting solids.

When this method has been used to create solids, another step is necessary to convert the solids to a 3-D computational mesh. The user must decide how many layers of mesh elements are required for each material layer solid. In cases where the layers pinch out or where the relative thickness of the layers varies, this can be confusing.

## Improvements to horizons method

With the release of GMS v6.0 in 2005, the development team updated the horizons method with several improvements, which were useful in creating the Allegan County mesh. First, the ability to assign horizons to TINs (in addition to boreholes) and to use both together to define the geology gives the user more control over the material contacts. Secondly, the tool to convert directly to a 3-D mesh from the solids prevents confusion associated with layer assignments and allows material sections to smoothly pinch out.

## Horizons and TINs

Previous versions of GMS only allowed the use of boreholes for assigning horizon numbers. This caused several problems in the Allegan County mesh. First, almost all of the borehole information was located on the bluff face. The section behind the bluff was assumed to be made up of distinct, flat, and continuous layers matching a single rotosonic borehole. To incorporate this assumption, extra boreholes were added throughout the model to force the interpolation to flatten out the layers. Even with the extra boreholes, though, the areas between the real boreholes and the dummy boreholes did not act as required because of the limitations of the interpolation techniques.

Without TINs, it was also difficult to incorporate the 4-ft-thick section of "smear" material. The material could be incorporated into the boreholes on the bluff face, but it often showed up in other areas of the model because of noise in the interpolation results.

The final mesh was created using the tools for assigning horizons to both boreholes and TINs in GMS v6.0. The boreholes (shown in Figure 4) were on the bluff face and were based on cross-sectional information (Personal communication, Dr. Ronald Chase, Western Michigan University). The borehole information was based on knowledge from the installation of the extraction wells, piezometers, and inclinometers. Two TINs designated the top and bottom of the smear zone (see Figure 5). They were interpolated from scatter points created from the original borehole information. The set at the bottom of the smear zone was simply offset 4 ft down. Where no smear material was found, the smear TINs extended up above the ground surface. These TINs were given horizon IDs just lower than those in the boreholes.

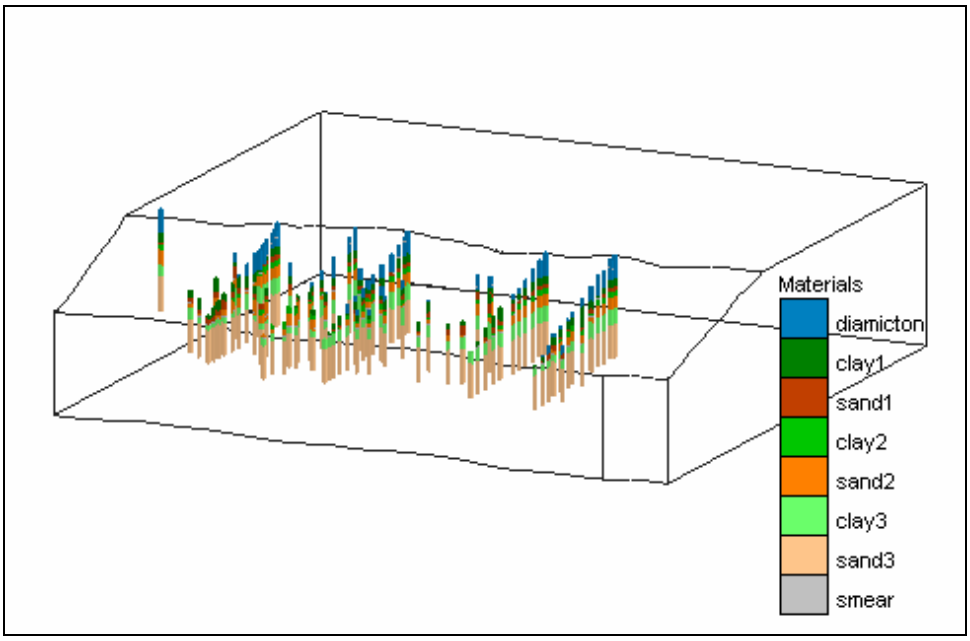


Figure 4. Boreholes from borings and cross-section drawings.

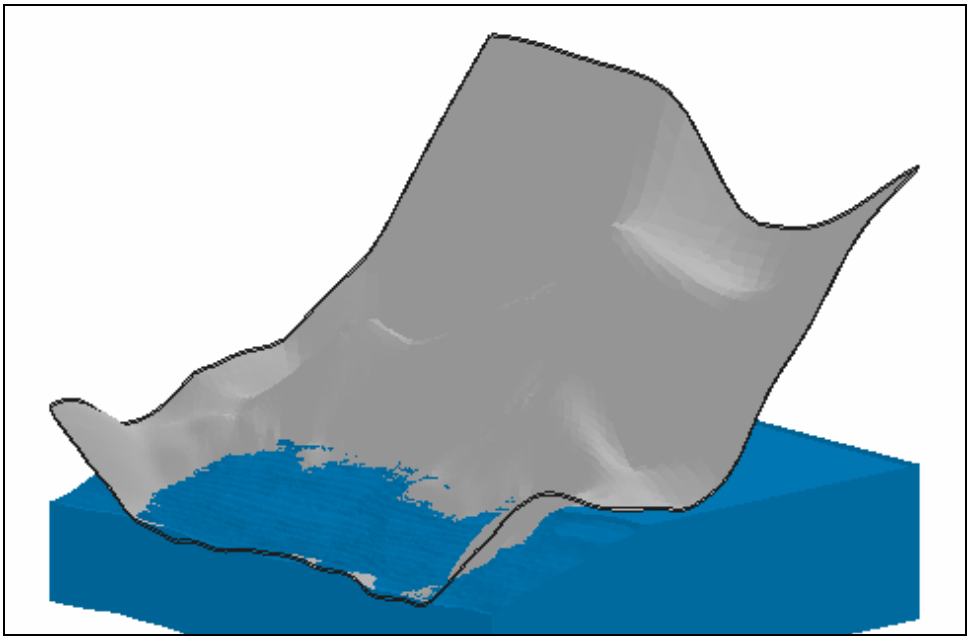

Figure 5. Two TINs (gray) represent top and bottom of the smear zone. In areas where there was no smear zone, the TINs were interpolated to be well above the ground surface and so, were ignored in making the mesh.

The flat, continuous layers existing behind the bluff face were created from the bottom smear zone TIN by using the Data Calculator in GMS. The TIN was duplicated and then every value larger than the top elevation of a specific layer was truncated. This resulted in TINs that exactly matched the smear zone, but flattened out behind the bluff face to delineate the

layering there. These TINs (shown in Figure 6) had the smallest horizon IDs.

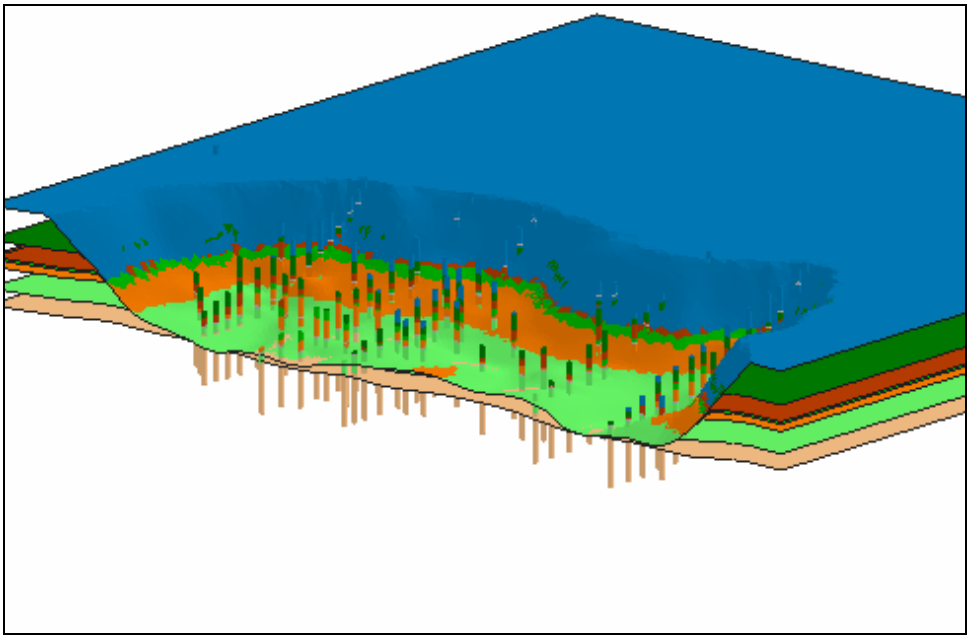

Figure 6. The boreholes and TINs used to define geological material distribution (TINs used to delineate smear zone have been hidden to allow a view of the other TINs).

Once the TINs and boreholes were entered with the correct horizon IDs, GMS was able to create a 3-D mesh in a single step based on a set of user-defined parameters including a minimum thickness for elements and the maximum number of elements placed between each set of horizons. The final mesh is shown in Figure 7 and Figure 8. It has 124,786 nodes and 693,691 tetrahedral elements.

## Mesh quality issues

The tools previously described are new, and although they have been thoroughly tested on a good range of problems, they do not seem to be robust enough to make a high quality mesh for this particular model. A quick analysis of aspect ratios shows that there are many poor-quality elements. In defense of GMS, this is arguably a difficult meshing problem. The mesh is adequate to be run in ADH, but it runs slowly. Some unsuccessful attempts were made to smooth the mesh. In the future as the horizon meshing technique matures and improves, a better mesh might be created.

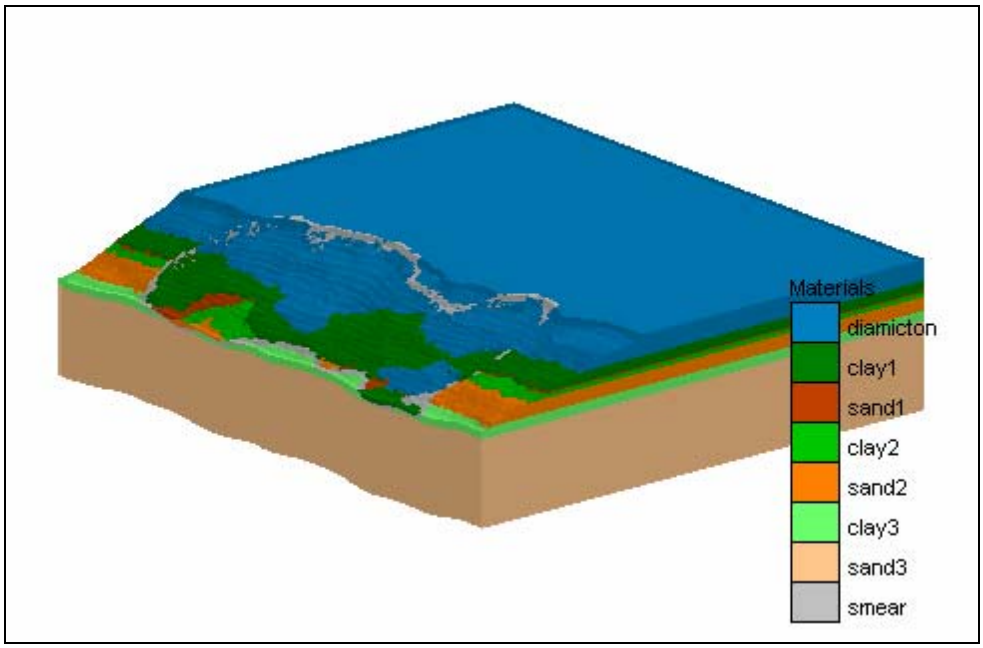


Figure 7. Finished computational mesh with material types assigned.

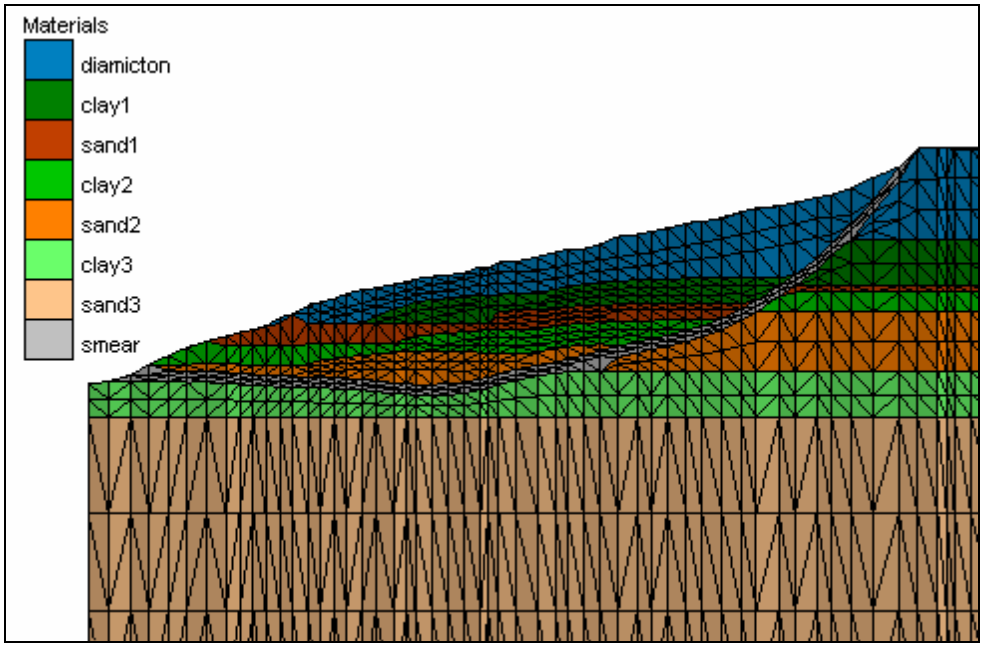


Figure 8. Typical cross section of finished computational mesh.

# 6 Model Boundary Conditions

The boundary conditions were set assuming flow is perpendicular to the shoreline. The western boundary is a specified head boundary condition set at 580 ft, an average elevation for lake level. The eastern boundary also has a specified head, but each of the water-bearing zones has a slightly different head value. The calibration period began with the upper diamicton zone having a head of about 671 ft. There were two lower sand layers that had heads of 594 ft and 595 ft. These boundary conditions were not based on measurements, so they will be altered during the steady-state calibration until the heads in the standpipes match the measured values. The specified heads on the intervening aquitards were interpolated between the aquifer heads. No boundary conditions were set on the north and south ends of the model because flow was assumed parallel to these boundaries. With no boundary conditions applied, no water was allowed to enter or leave the model through these edges.

The top ground surface of the model had a small recharge value applied as a flux boundary condition. The bluff face was set with an exit face boundary condition. This type of boundary condition was set by switching on the option to model groundwater-surface water interaction and then forcing the surface water depth to be zero. This allowed water to exit the face when the pressure head behind the bluff face is greater than zero. This water disappeared from the model because of the zero depth boundary condition (corresponding to flowing down the cliff to join the lake water). If the pressure behind the bluff face is negative, no interaction occurs between the surface water and the groundwater.

Although the horizontal well, near the top edge of the bluff, was actually a groundwater sink, it was modeled as a boundary condition. It was basically a French drain, so it was represented by a line of nodes at or near the surface with specified heads equal to the elevation of the pipe. When the head in the surrounding soil was greater than that specified, water left the model until the heads along the drain were equal to the pipe elevation. This essentially forced the water table to pass through the pipe.

Several source/sinks were included at interior locations of the model. All three of the standpipes near the middle of the domain were incorporated as sources, but were only activated during the transient calibration stage. There were no pumps on these standpipes, so they were modeled as

specified heads at the interior nodes along the standpipe screens during the period when water was added to the standpipes. This setting will be removed at that point to calibrate the recovery period.

All of the bluff-face dewatering wells were added to the model as sinks. They will be turned on after calibration to determine the success of the dewatering scheme. These are modeled with flux terms applied to a node or column of nodes at the locations of the well screens.

# 7 Calibration

A calibration process was used to determine model parameter values that best reproduce the conditions existing at the site in May 2004. The parameters, which were varied, included the upstream head boundary conditions and the hydraulic conductivities and storage coefficients for all eight materials.

## Calibration data

The best data available for calibration was from modified slug tests run in three screened standpipes located about 75 ft back from the bluff face. All three standpipes had a diameter of 2 in. The shallowest of the standpipes had a screen beginning 19 ft below the ground surface continuing up to a point 13 ft below the ground surface. This placed the screen in the diamicton till layer. At the time the tests were performed (May 2004), the head in this layer was almost at ground surface – in fact, the top of the water surface could be seen from the top of the pipe.

The middle standpipe had a screen beginning 86 ft below the ground surface up to 65 ft below the ground surface. This screen was placed mostly in the middle sand layer. The deepest standpipe had a screen 129.5 ft below the ground surface up to 94.5 ft below the ground surface. This was screened mostly in the deep sand aquifer, which was connected to the lake. The locations of each of the screens with respect to the geologic layers are shown in Figure 9.

A flow meter was connected to the end of a hose, and the water was turned on full for about a half an hour in the deep and middle standpipes. The flow rate averaged just less than 4.5 gal/min. At several points during the test, the time and flow meter readings were recorded. This was used to calculate the flows from the hose during the test. Figures 10 and 11 show the data from the flow meter and the average flow rates marked halfway between each flow meter reading.

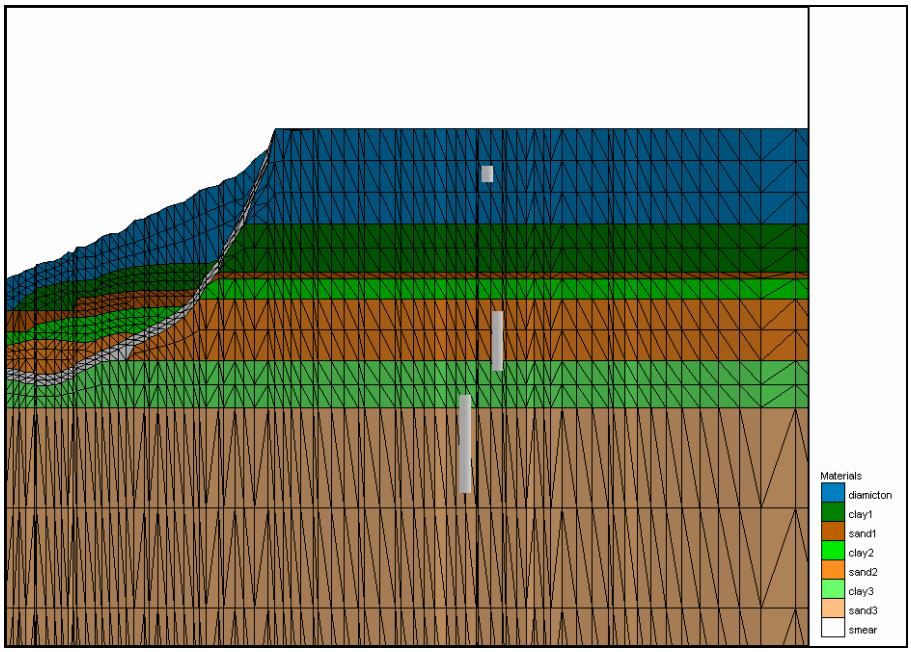


Figure 9. Locations of three standpipe screens in the model.

There was also an immersible water level logger (Levellogger) in each standpipe before, during, and after the pumping period to measure the response. These data are shown in Figures 12 and 13. In both tests, the head increased rapidly when the water was first turned on and quickly reached a steady-state condition where the water flowing into the pipe from the hose was matched by the water leaving the standpipe and flowing into the surrounding aquifer. The head remained constant until the water was turned off and then quickly dropped with an immediate steep slope gradually flattening until the water level reached its previous elevation asymptotically.

A similar test was run in the shallow standpipe. However, because the water level was so close to ground surface, the standpipe overflowed almost as soon as the water was turned on. The test happened too fast to be able to get an accurate reading from the flow meter, so the flux information is not accurate enough for calibration. The immersible data logger, however, accurately logged the recovery period (Figure 14), so transient calibration to the water levels can be applied to the diamicton layer.

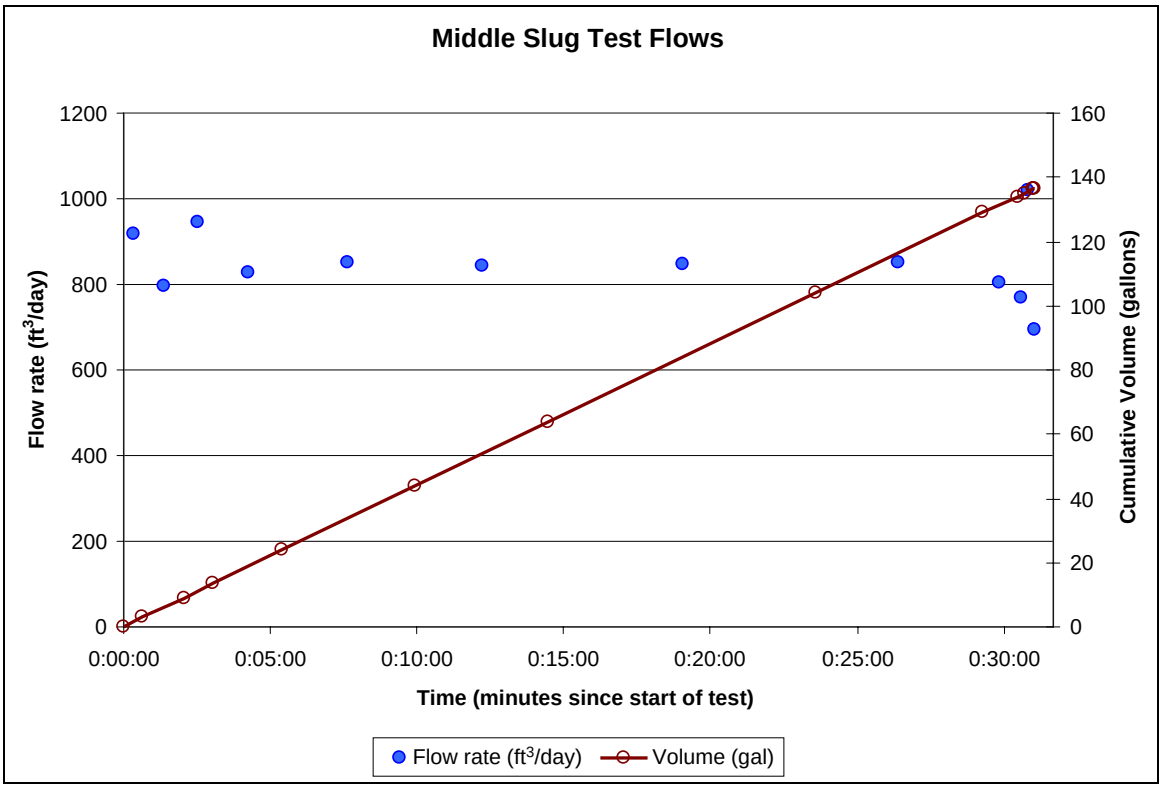


Figure 10. Flow information for middle standpipe slug test.

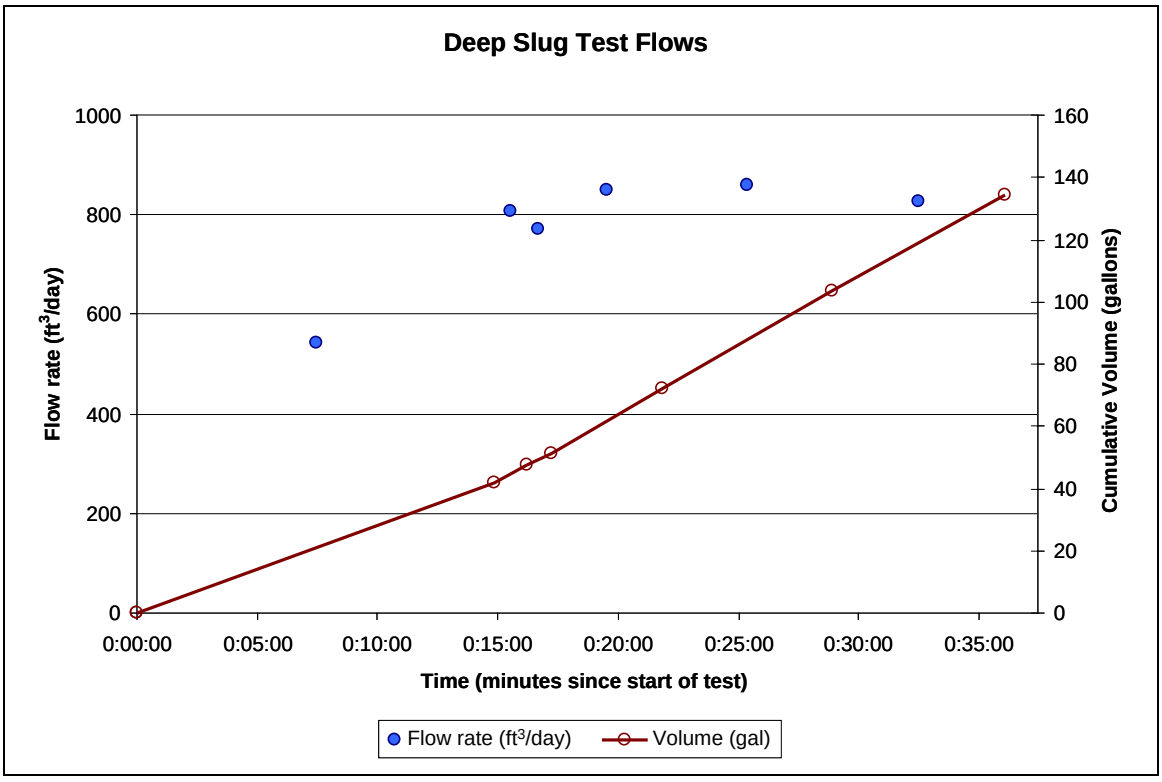


Figure 11. Flow information for deep standpipe slug test.

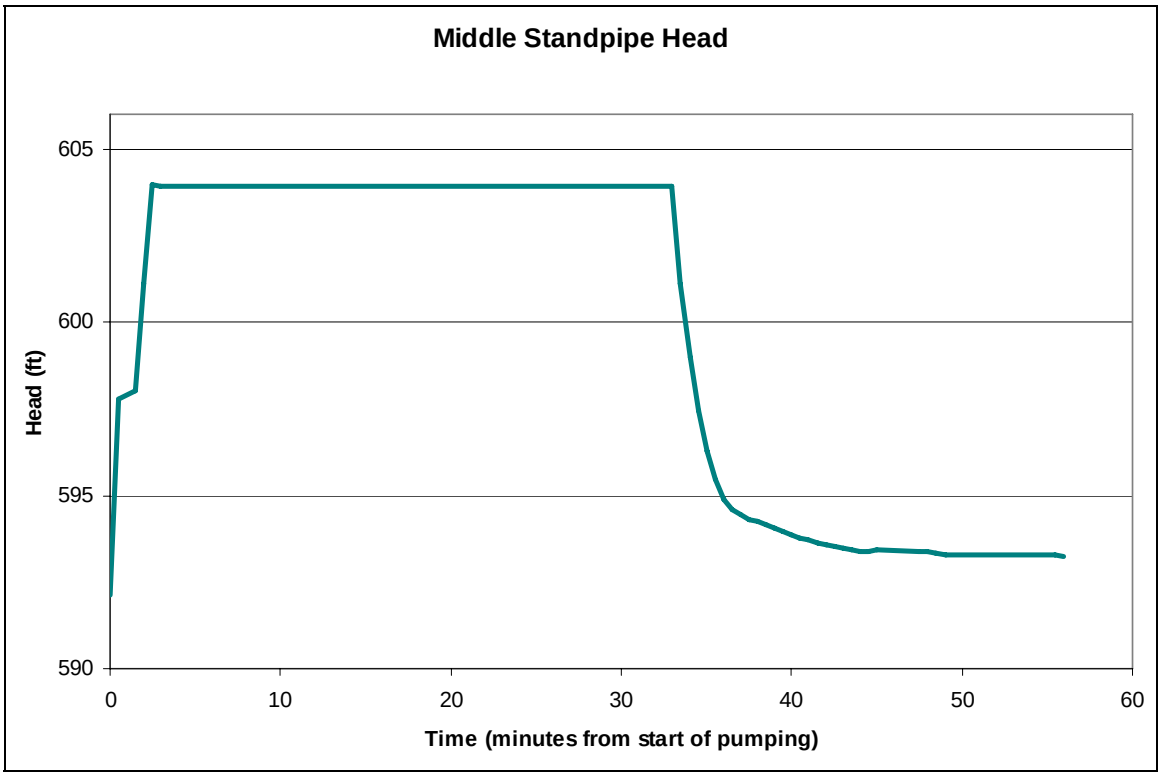


Figure 12. Head measurements from Levellogger during and after slug test in middle standpipe (one reading every 30 sec).

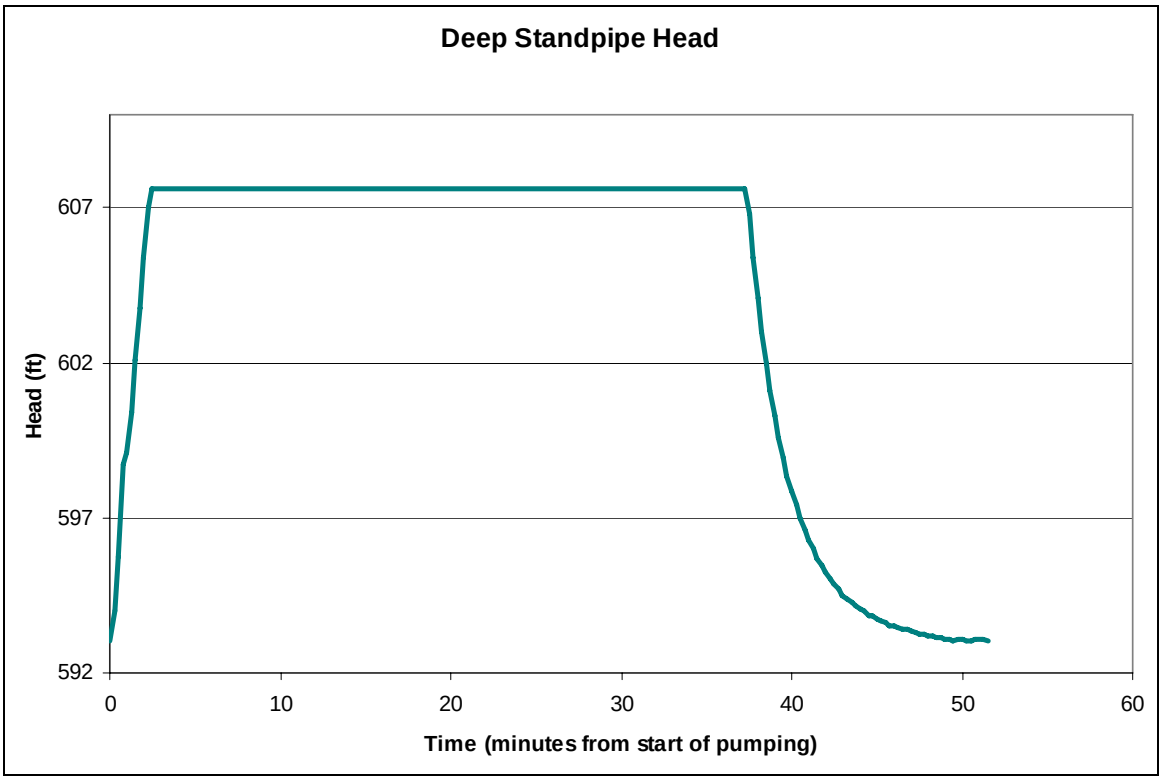


Figure 13. Head measurements from Levellogger during and after slug test in deep standpipe (one reading every 15 sec).

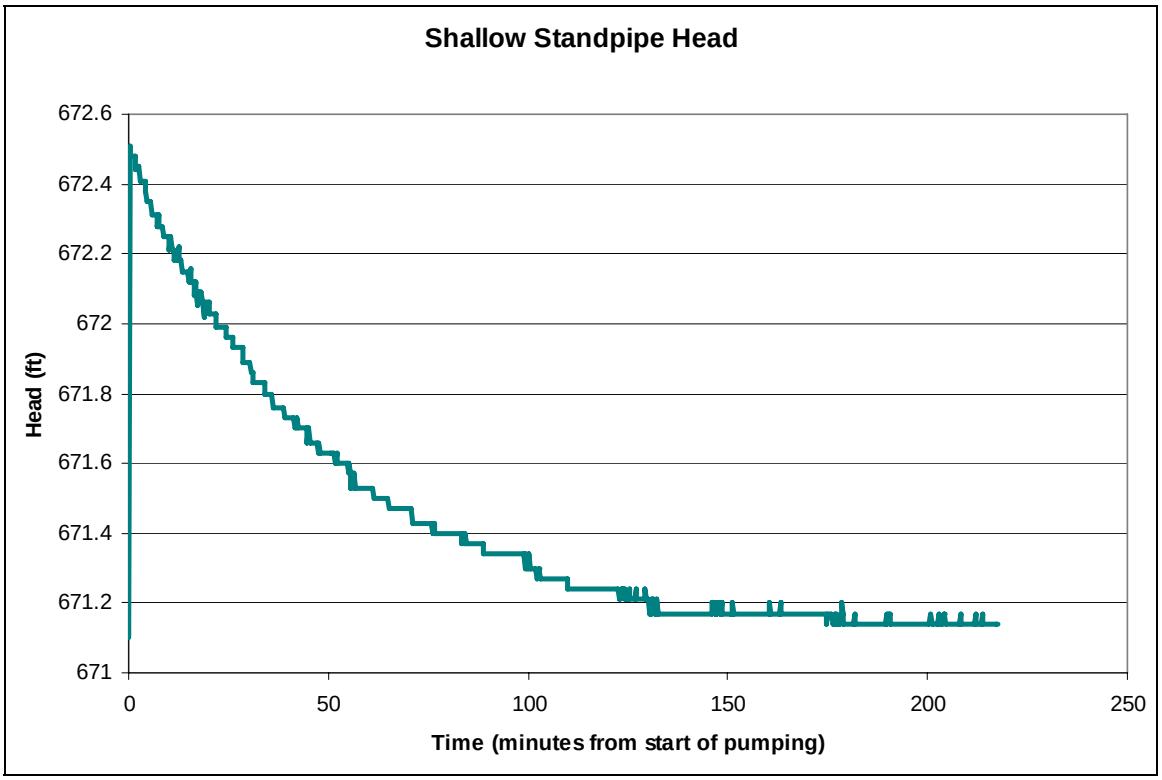


Figure 14. Head measurements from Levellogger during and after slug test in shallow standpipe (one reading every 15 sec). Note: Plot seems blocky and jagged because logger was set to record only two decimal places for head values.

## Calibration procedure

The calibration process was to estimate:

- upstream boundary conditions using the steady-state water level data
- hydraulic conductivities using the steady-state water level data and the transient flux data from the slug tests
- storage coefficients with transient water level data from the slug tests.

It is important to use heads and fluxes to calibrate a model such as this with only specified head boundary conditions. For such models, any multiple of the correct conductivity values should yield the same head results. For example, if every conductivity value were 10 times the "correct" value, the heads would still match up. The fluxes, however, would be significantly different. Using heads and fluxes for calibration yields a valuable, calibrated model.

Because the hydraulic conductivities were being calibrated both with the steady-state water level data and the transient flux data from slug tests,

the process was iterative. This required several passes to converge to a single set of conductivity values that fit both data sets.

## Calibration to steady-state water levels

The first step of the calibration process was to match the static heads measured in the three standpipes. These heads were measured during a site visit in May 2004 and were fairly constant over the week, except for during the pump tests. The upstream head boundary conditions and the conductivity values for each material were the parameters that were varied during this process. Initial conductivity values were estimated since there is limited data available.

The upper standpipe is screened entirely in the upper diamicton layer. It is sensitive both to the upstream boundary condition and the ratio between the conductivity values in the diamicton and the smear materials. If the two materials have conductivity values that are too similar, the water does not back up behind the bluff face and the water table drops off too soon, making it impossible to replicate the high head that was measured in the top standpipe. The process showed that the smear must have a small conductivity comparable to the diamicton.

The topological data obtained for the model only included the survey data from the bluff face. Because of a lack of data, the mesh was built with the inaccurate assumption that the ground surface was perfectly flat from the edge of the bluff back to the upstream edge of the model. As a result, the upstream head boundary condition had to be set higher than the top of the mesh in order to match the measured head in the top layer. This does not, however, affect any other results in the model.

The middle standpipe is screened in the second sand layer. The head in this layer was somewhat affected by the ratio between the conductivity of the sand and that of the smear, though, not to the same extent as with the diamicton. The greatest effect on this layer is exerted by the upstream specified head boundary condition.

The bottom standpipe is screened in the lowest sand layer at about the level of the lake. Because this layer is mostly below the smear zones and we are specifying heads on both ends, this layer was not very sensitive to the conductivity value. It was fairly easy to match the head in this standpipe by varying the upstream specified head.

Table 1 compares the measured heads in each of the standpipes and the calibrated model result. The model output is visualized in Figure 15 with the saturated zones denoted with a transparent blue color over the geology.

Table 1. Results for steady-state calibration.

| Material | Measured Head ft | Calibrated Model Head, ft | Residual, ft |
|---|---|---|---|
| Diamicton | 671.1 | 671.17 | 0.07 |
| Sand 2 | 592.2 | 592.79 | 0.59 |
| Sand 3 | 593.04 | 593.23 | 0.19 |

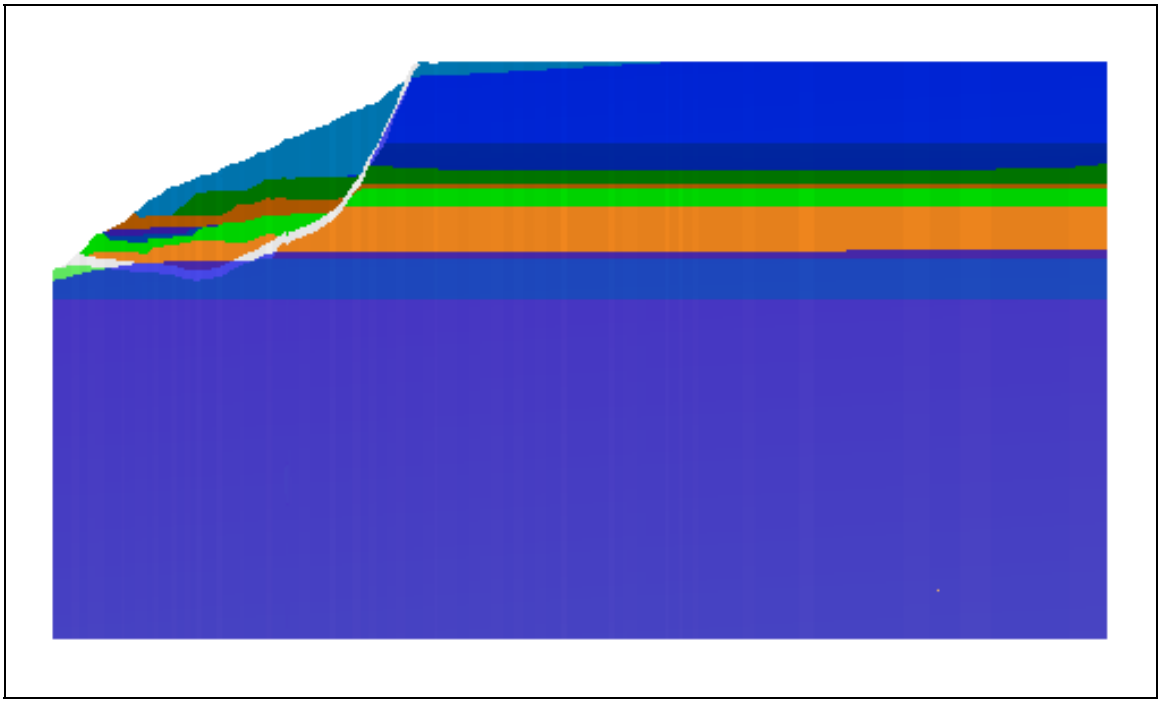

Figure 15. A typical cross section of bluff with saturated sections overlain as transparent blue sections.

## Calibration to transient fluxes

The first part of the transient calibration is to verify the conductivity values by running the model with the head specified in the standpipe according to the measurements during the pumping period of the test. ADH writes out the flux rate at every specified head node for every time-step. This is then compared to the flux calculated from the flow meter data during the test. The calculated fluxes are highly sensitive to the conductivity values.

The model runs for reproducing the pump period of the slug tests were set up to run from the time the water was turned on until the time it was turned off. A specified head boundary condition was set at each of the mesh nodes within the standpipe screen and the head was set with the plots shown in Figure 12 and Figure 13 (with the recovery period removed). When the model was finished, the flux output file was read into GMS and the flux values at each of the screened nodes were extracted. In both cases, more than one mesh node fell within the screen length, so the flux values were summed and then compared to the fluxes calculated from the flow meter on the hose (shown as blue points in Figure 10 and Figure 11). The conductivity values were altered until the flux values were similar to those measured in the field. Figure 16 and Figure 17 show the comparison between the model calculated flux and the measured field flux with the calibrated parameter values.

## Calibration to transient water levels

The final step in the calibration process was to calibrate the storage coefficients by comparing the model calculated recovery after the slug tests, to the recovery recorded by the immersible data loggers. The recovery after the pumping into the middle and deep standpipes were previously shown in Figure 12 and Figure 13. See Figure 14 for a similar plot for the shallow standpipe.

With the upstream heads and conductivity values set from previous calibration efforts, the storage terms were altered to find the best fit to the recovery plots for each of the tested layers. It turned out to be difficult to match the recovery plots as closely as desired. The differences are probably the result of local heterogeneities that were not included in the model. Rocks, cracks, fissures, and plant material can affect the flow characteristics, but cannot be included in a model on this scale.

The calibrated results are shown in Figure 18 through Figure 20.

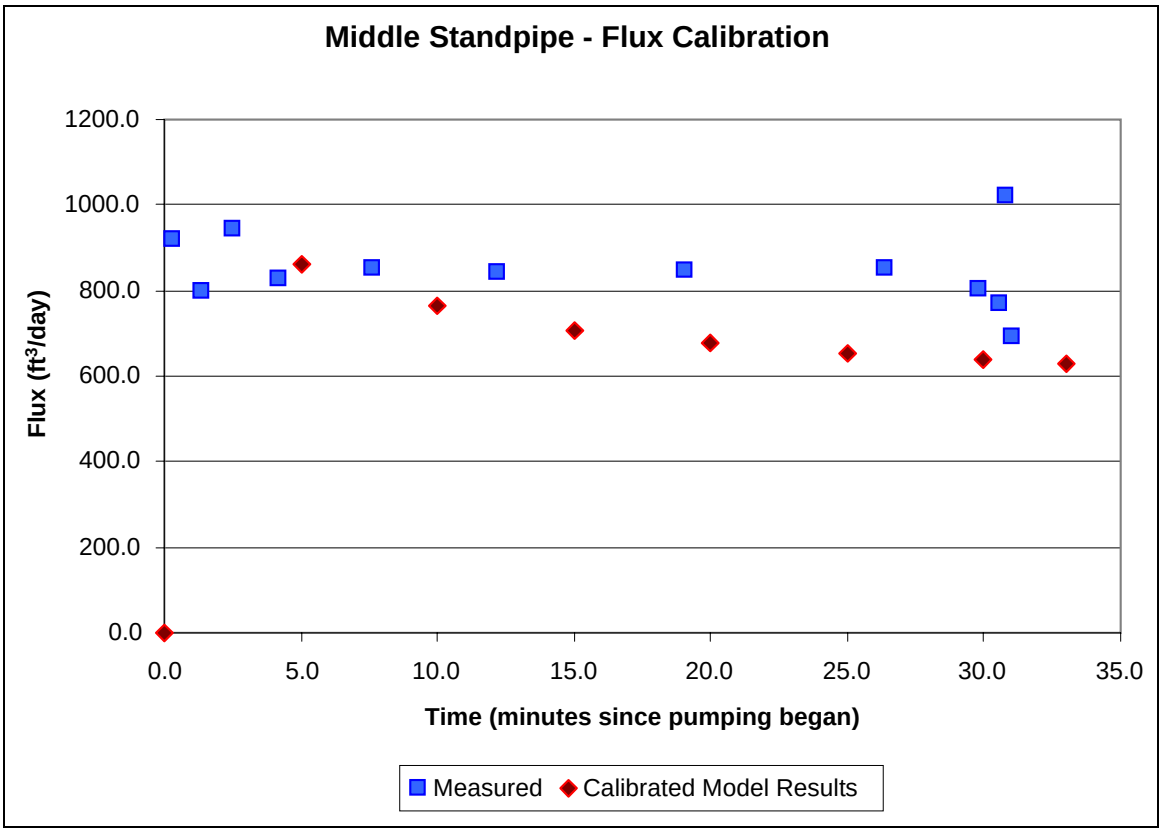


Figure 16. Calibration results for flux calibration in middle standpipe.

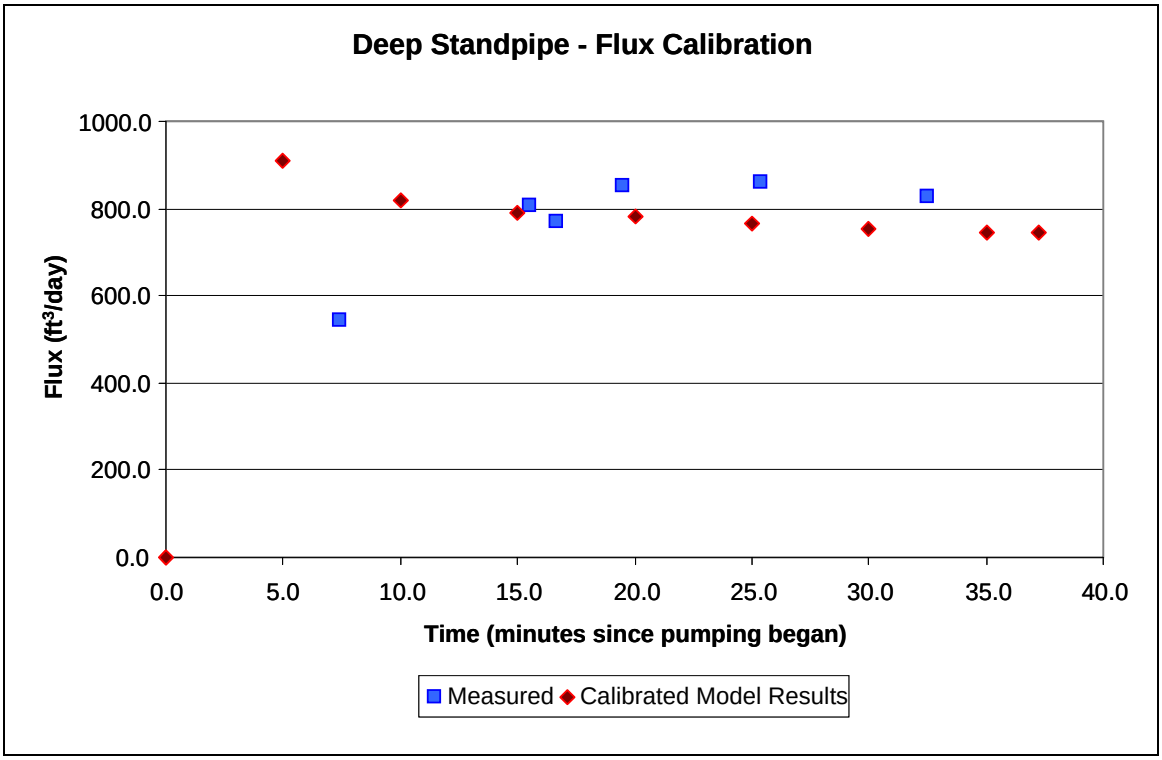


Figure 17. Calibration results for flux calibration in deep standpipe.

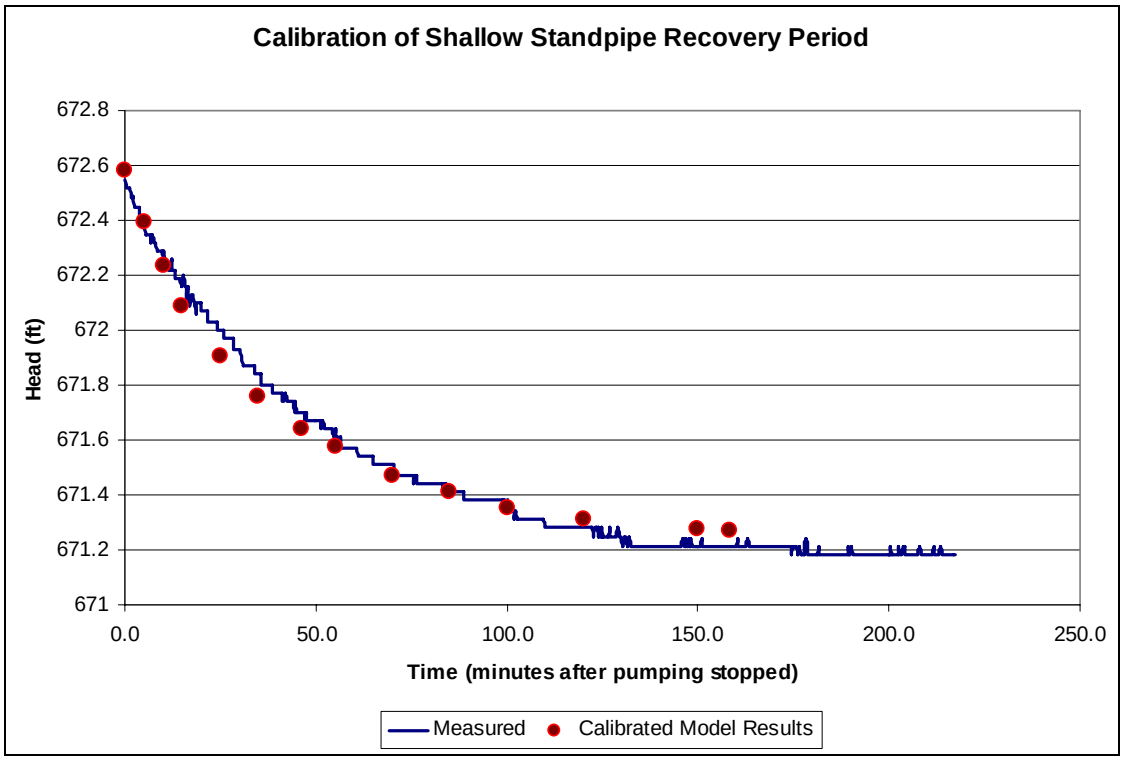


Figure 18. Calibrated model output compared to measured head values during pump test recovery period in shallow standpipe.

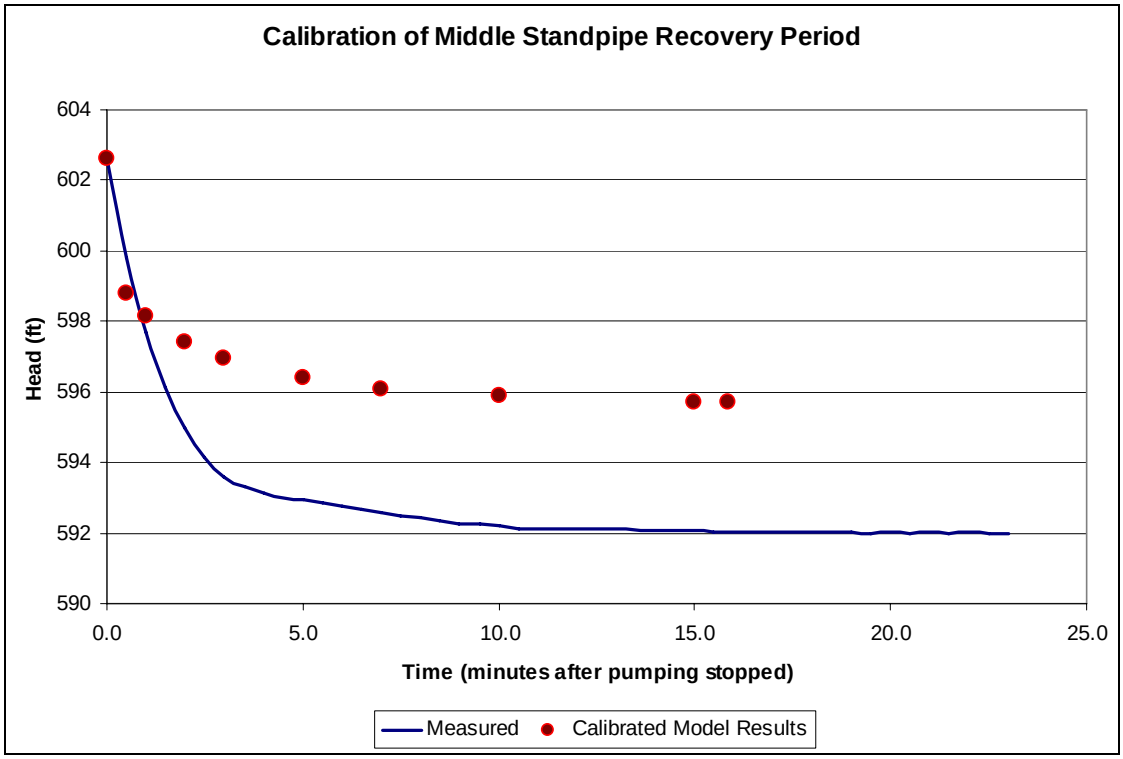


Figure 19. Calibrated model output compared to measured head values during pump test recovery period in middle standpipe.

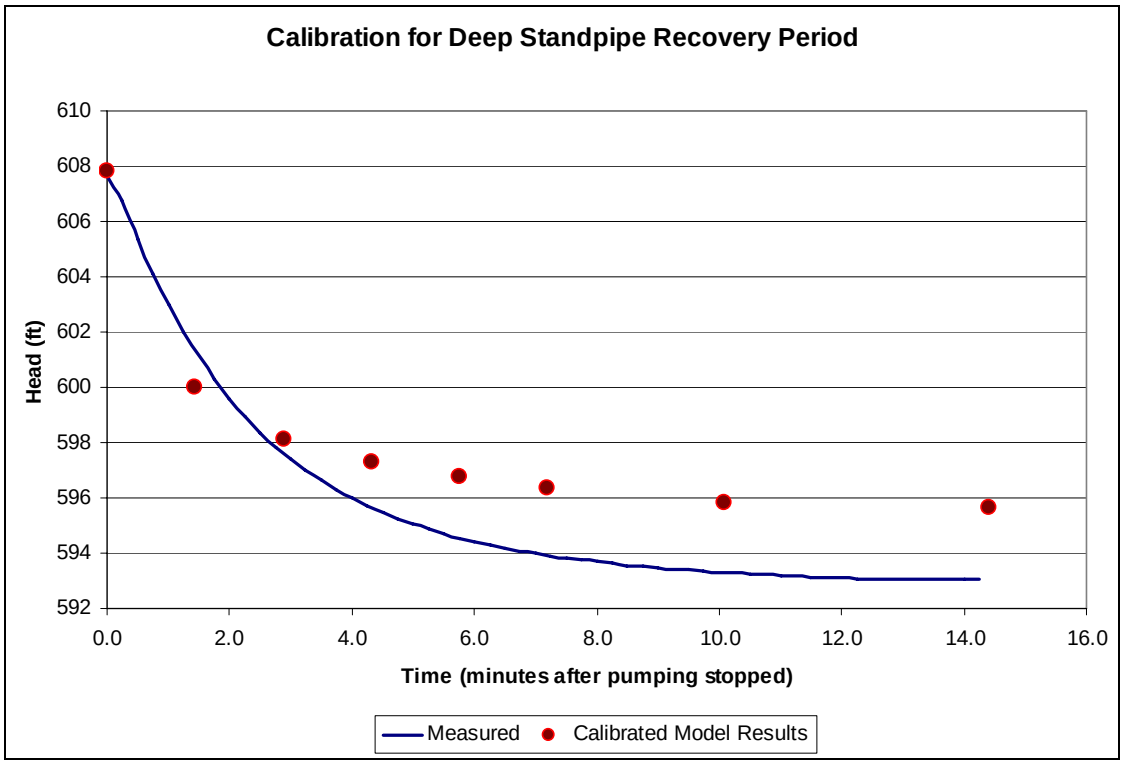


Figure 20. Calibrated model output compared to measured head values during pump test recovery period in deep standpipe.

## Calibration results and analysis

The final selections for the parameter values based on the calibration results are listed in Table 2. Most of the values are within accepted ranges for the material types. The diamicton conductivity and storage values seem too high for a clay-rich till, but the values are probably accurate because of sand-lined shrinkage cracks, which increase the conductivity. Further, because this is the surface material, it could easily be affected by rocks, plant matter, human activities, etc. Vertical cracks are visible in the upper diamicton and have been studied and documented (Chase 2001a, 2001b).

Table 2. Final calibrated parameter values for the model.

| Material | Horizontal Hydraulic Conductivity, ft/day | Vertical Hydraulic Conductivity, ft/day | Specific Storage unitless | Upstream Specified Head, ft |
|---|---|---|---|---|
| Diamicton | 4.0 | 40.0 | 4.0e-2 | 682.0 |
| Clay 1 | 0.001 | 0.0001 | 1.0e-4 | 631.0 |
| Sand 1 | 28.3 | 28.3 | 1.0e-5 | 580.0 |
| Clay 2 | 0.001 | 0.0001 | 1.0e-4 | — |
| Sand 2 | 40.0 | 40.0 | 1.0e-4 | 593.0 |
| Clay 3 | 0.0001 | 0.0001 | 1.0e-4 | 598.5 |
| Sand 3 | 0.7 | 0.7 | 1.0e-6 | 604.0 |
| Smear | 0.0001 | 0.0001 | 1.0e-4 | — |

With the exception of the middle pump test recovery, and to a lesser extent the deep pump test recovery, the comparisons between the model results and the field-measured data are encouraging.

In addition to the good similarity between field measurements and model output, the model also correctly predicts seepage locations on the bluff face as shown in Figure 21. Seepage areas occur at the bottom of a conductive layer when underlain by a nonconductive layer.

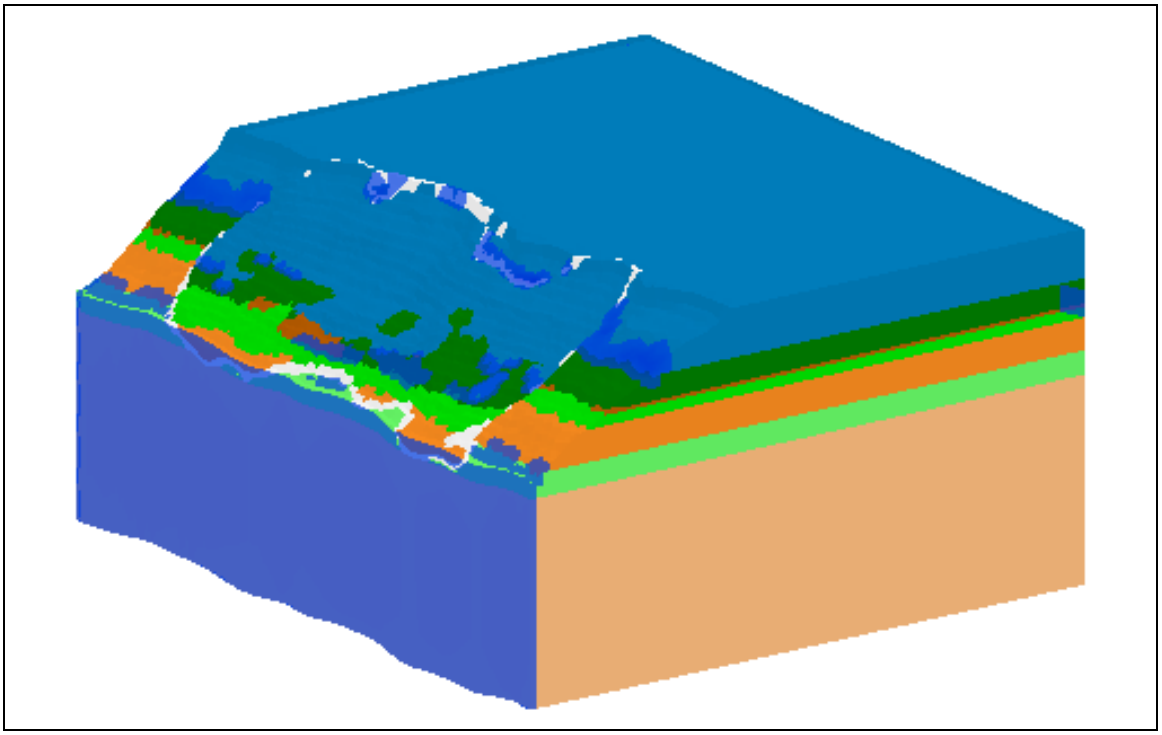

Figure 21. Allegan County mesh overlain with a transparent blue color indicating locations of exiting fluxes.

Figure 22 shows the degree of saturation in the model. Blue areas are completely saturated while red areas are almost completely dry. The green and yellow areas are partially saturated. Again, the bottom sections of the conductive materials are completely saturated when they are underlain by a nonconductive material.

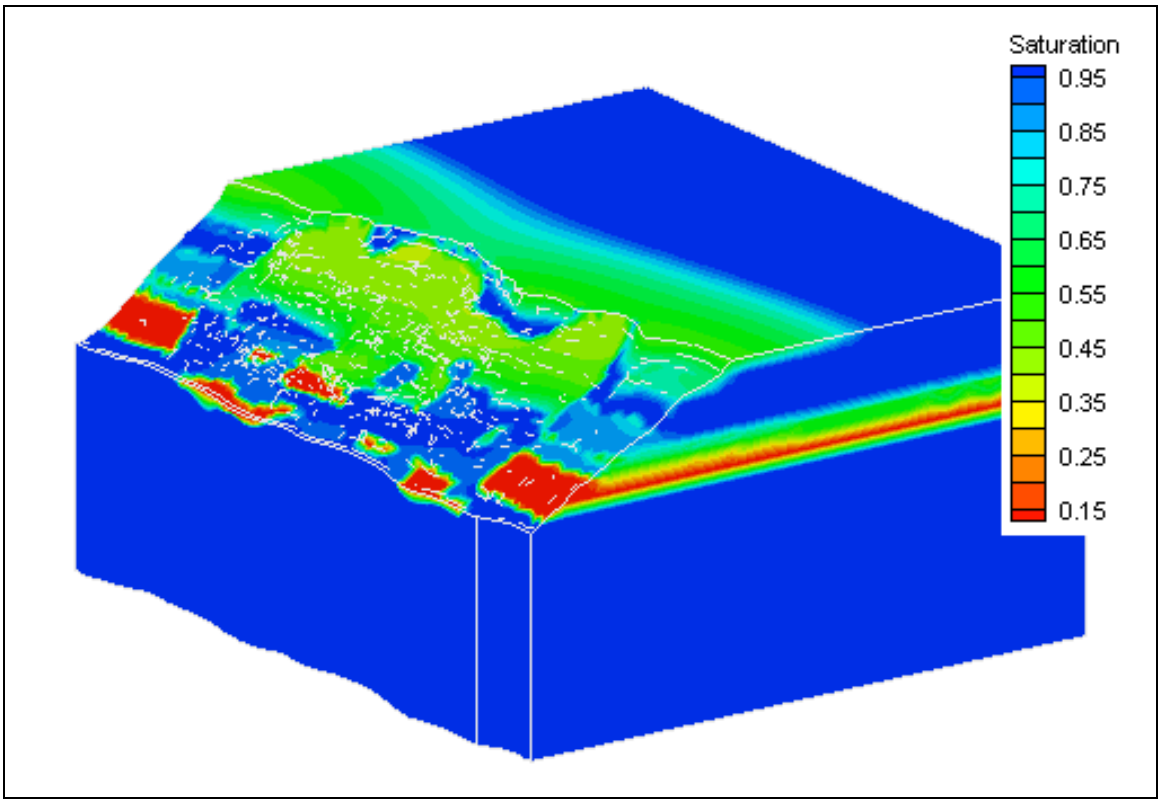


Figure 22. Allegan County model with contours indicating degree of saturation (blue areas are completely saturated; red areas are completely dry).

# 8 Final Run with Dewatering

Armed with a calibrated model, the next step was to turn on the dewatering equipment in the model to view the results on the entire system. This site contains both a horizontal well and 17 traditional pumping wells.

## Horizontal well

The horizontal well is placed parallel to the bluff face just before the bluff drops off. The north end was placed 19 ft below ground surface and the south end is 21 ft below ground surface (see map location in Figure 23). The well works like a French drain with the water from the saturated soil seeping into the pipe when the head is higher than the pipe invert elevation. The water then flows downhill in the pipe to the south end where it connects to an exit pipe that takes the water partway down the bluff face and releases it to the lake.

Because there is no pump on this well and there is no device for measuring the amount of water removed, the horizontal well is best modeled as a string of specified head nodes. The head will be set at the invert elevation for the drain pipe. This will result in the removal of any water in those nodes above the pipe elevation.

The only drawback to this setup is the danger of the water level falling below the pipe elevation. If this happens, the model will continue to keep the water at the specified level, resulting in the addition of water through the drain. Because of the model setup with continuous addition of water on the west side of the model, this is not likely to happen, but the flux values at these nodes were carefully watched to be sure no extra water was introduced to the model in this way.

For simplification, the specified head was assumed constant for the whole pipe length instead of a linear interpolation between the north and south depths. Since the ground surface elevation at this location is 672 ft, the pipe elevations are 653 ft and 651 ft for the north and south ends, respectively. All the nodes on the line will be set to 652 ft. This simplification will have minor significance to the model results.

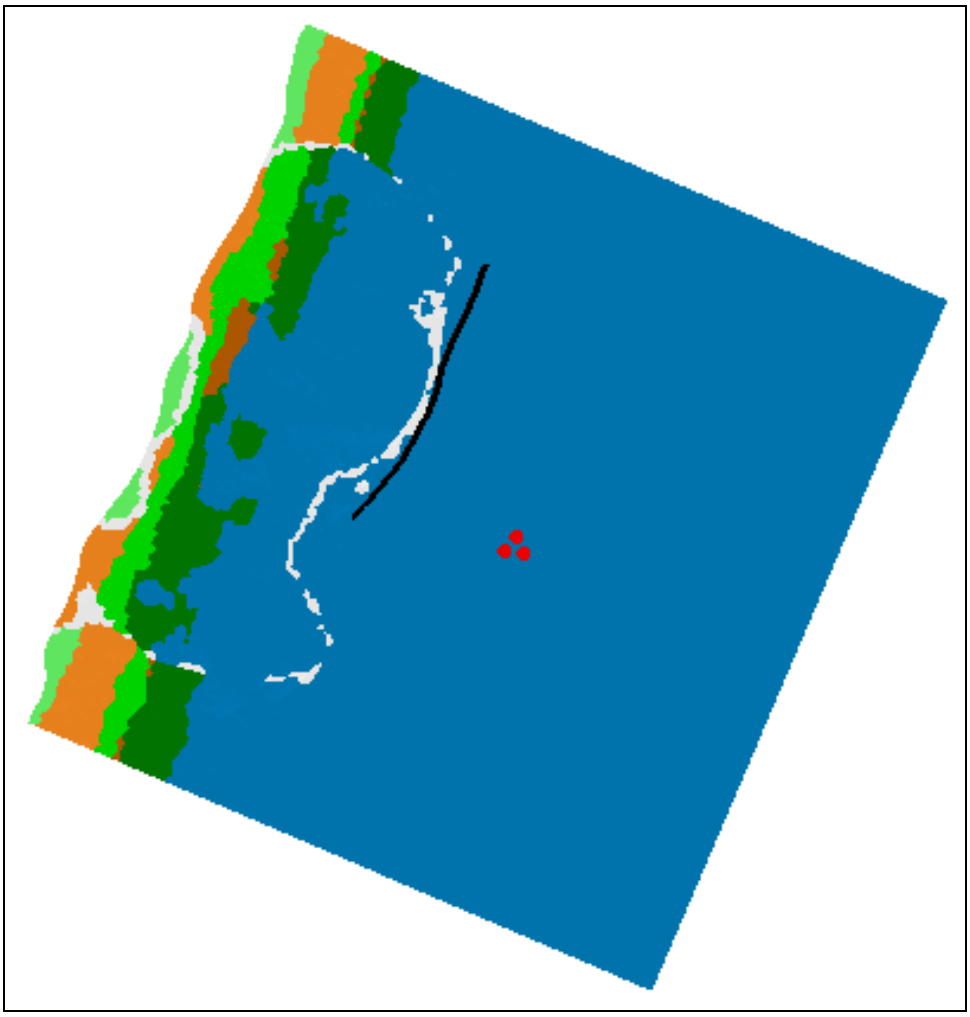

Figure 23. Horizontal well is denoted by the thick black line just back from the bluff (red dots indicate the locations of the three standpipes).

The spacing of the nodes in the vertical direction also becomes important. Because of the thickness of the diamicton layer and the parameters used to build the mesh, the second node down (directly below the surface node) is at an elevation of 660.7 ft. The third node is at an elevation of 649.4 ft. Thus, the top two nodes were selected for the specified head boundary condition because their elevations are above the pipe elevation. This results in a total of 78 nodes being set for the simulation of the horizontal drain.

The effect of the horizontal well is easily visible in a comparison between Figure 24 (degree of saturation before adding the horizontal well) and Figure 25 (degree of saturation after adding the horizontal well). The interface between the saturated ground surface and the drier ground surface is farther back from the bluff when the horizontal well is added.

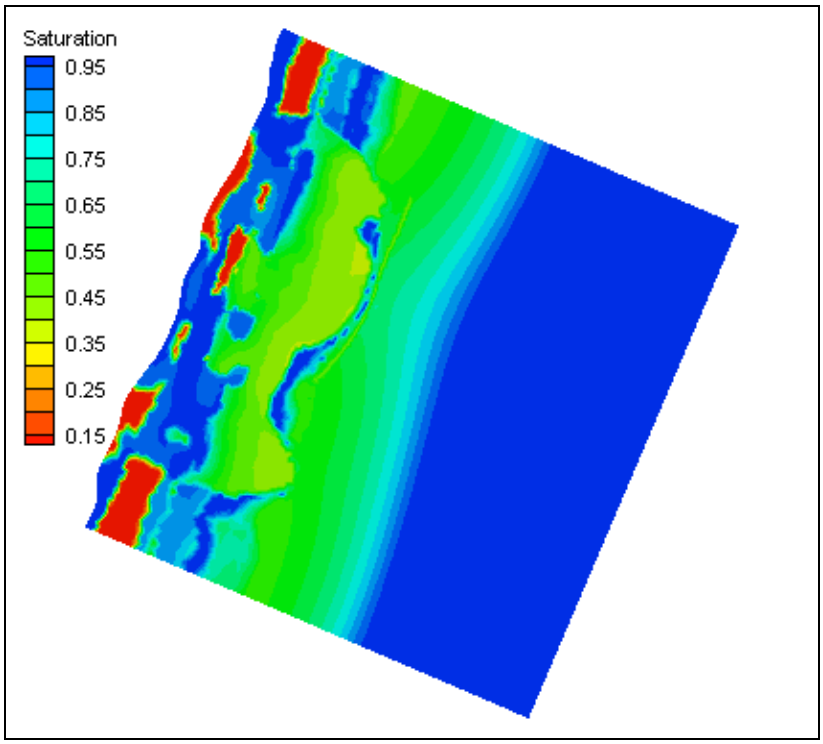


Figure 24. Plan view of model prediction before the addition of the horizontal well. Contours are for degree of saturation (blue areas are saturated; red areas are almost dry). Compare to Figure 25.

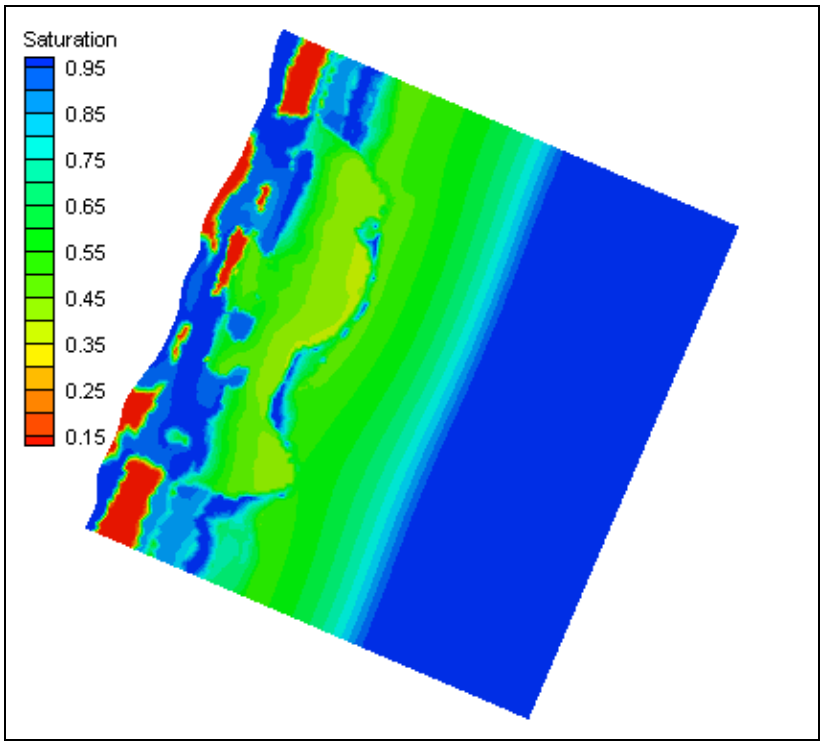


Figure 25. Plan view of model prediction after the horizontal well has been working for 100 days. Contours are for degree of saturation (blue areas are saturated; red areas are almost dry). Compare to Figure 24.

The dewatering effect of the horizontal well is also visible when viewed on a cross section. Figure 26 shows the model-predicted degree of saturation on a typical cross section perpendicular to the bluff. The effect of the horizontal well is apparent when compared to Figure 27, which shows the degree of saturation on the same cross section 100 days after the addition of the horizontal well. The less-saturated zone spreads to the right (away from the lake, and also extends downward somewhat. However, no difference is visible in the bluff face, on the lake side of the failure plane.

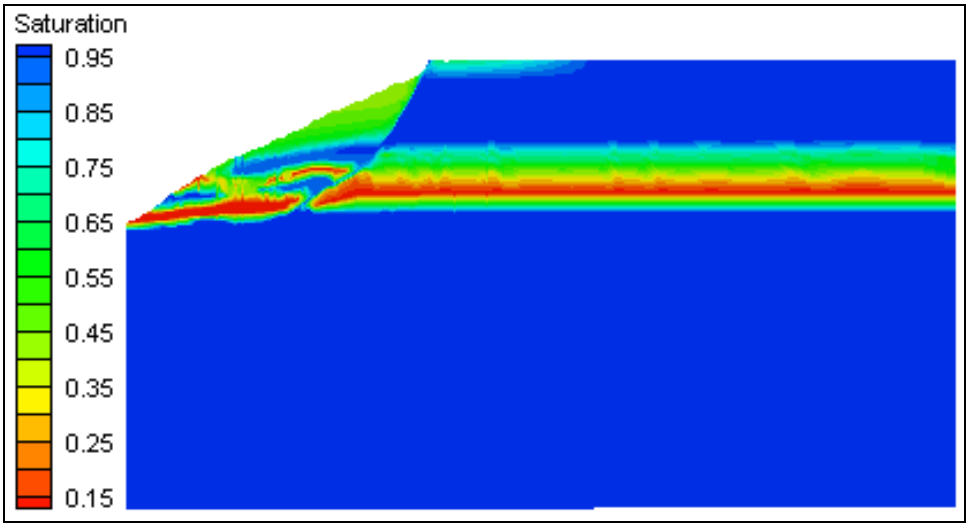


Figure 26. Model predicted degree of saturation on a cross section before insertion of horizontal well (blue areas are saturated; red areas are almost dry). Compare to Figure 27.

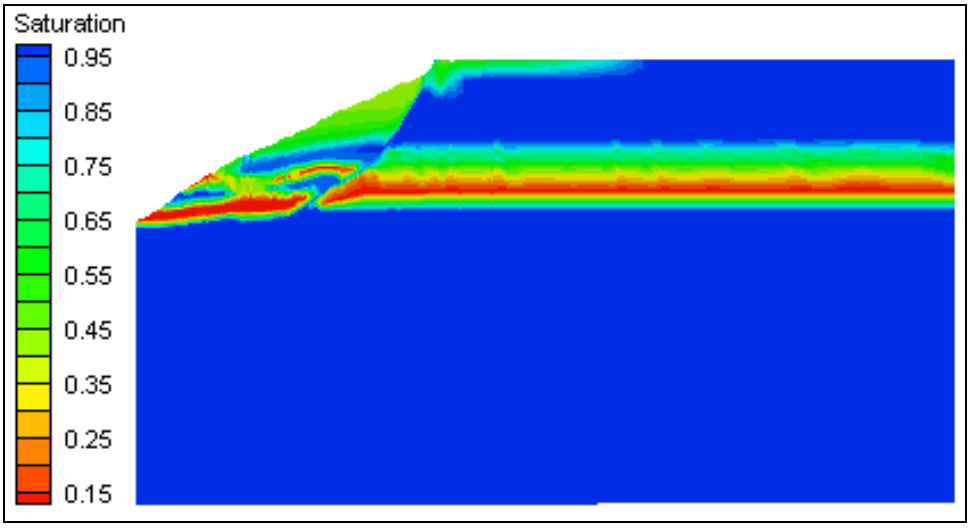


Figure 27. Model predicted degree of saturation on a cross section 100 days after insertion of a horizontal well (blue areas are saturated; red areas are almost dry). Compare to Figure 26.

## Pumping wells

The dewatering scheme also includes 17 pumping wells placed at various points below the bluff face. The surface locations are denoted with red dots in Figure 28. Each well was screened at a different depth as shown in Figure 29. The thick black section of the well column indicates the screened location.

These extraction wells were designed to turn on and off automatically, as the water level rises and falls. The pumps operate until the head in the well is 1 ft above the pump. At this point, the well stops pumping and sits idle until the head rises to 3.5 ft above the pump. Then, the pumping begins again until the water drops too low. The pump settings range from 7,000 to 10,000 rpm. All are set to the slowest rpm. Each well also has a flow meter attached.

During the site visit in May 2004, several pump tests were run on the wells that had water in them. All of the top tier wells (1, 4, 7, 10, 13, and 17) were dry. Most of the middle tier wells (2, 5, 11, and 15) were also dry. The only dry bottom tier well was 16. The other bottom tier wells (3, 6, 9, 12, and14) and middle tier well 8 all had enough water in them for pumping. See Figure 30 for well locations and clarification.

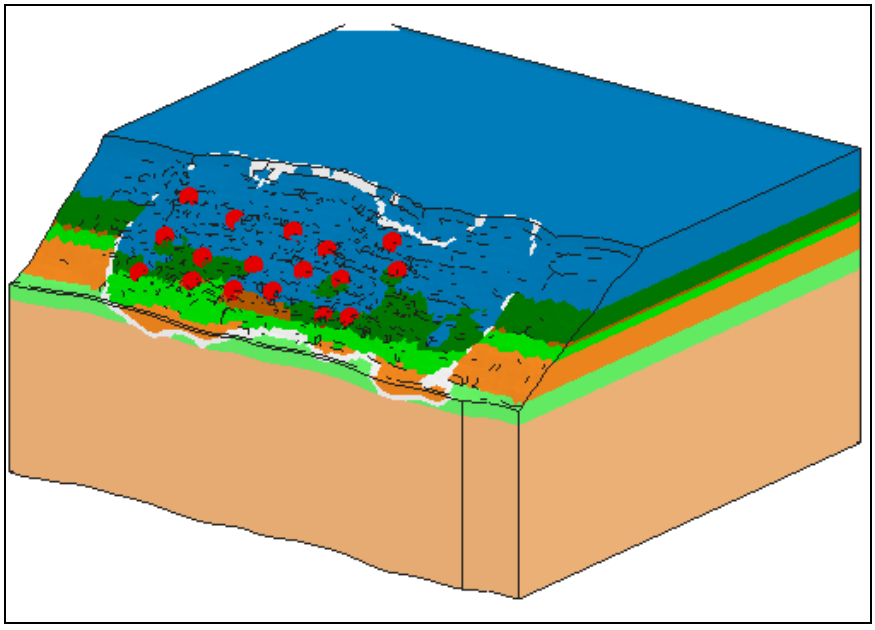

Figure 28. Locations of dewatering wells (red dots) on bluff face.

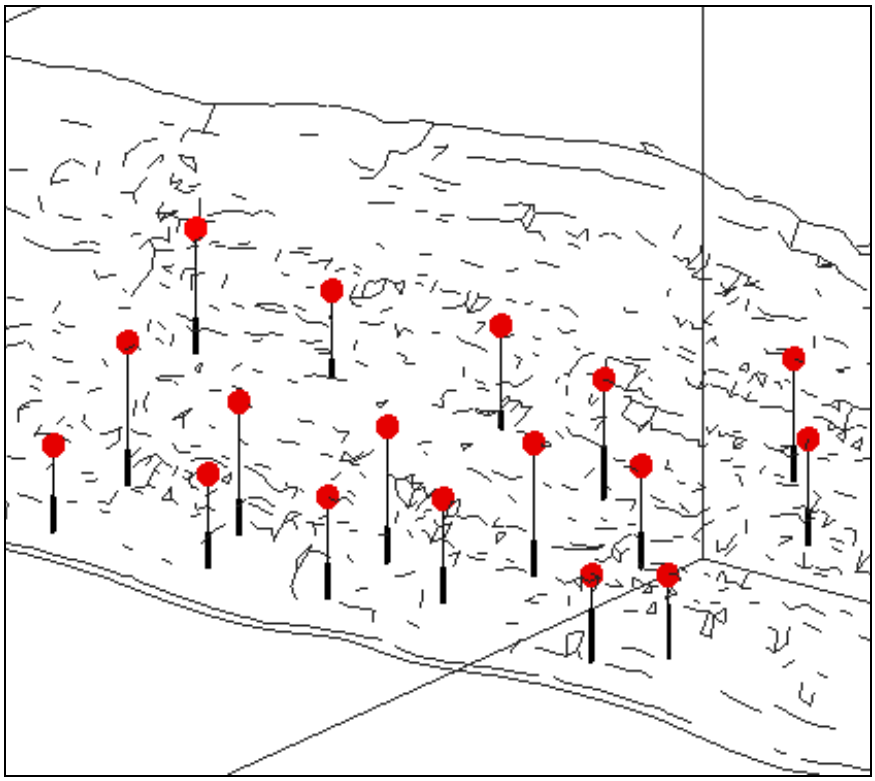

Figure 29. View of dewatering well screen locations in bluff face.

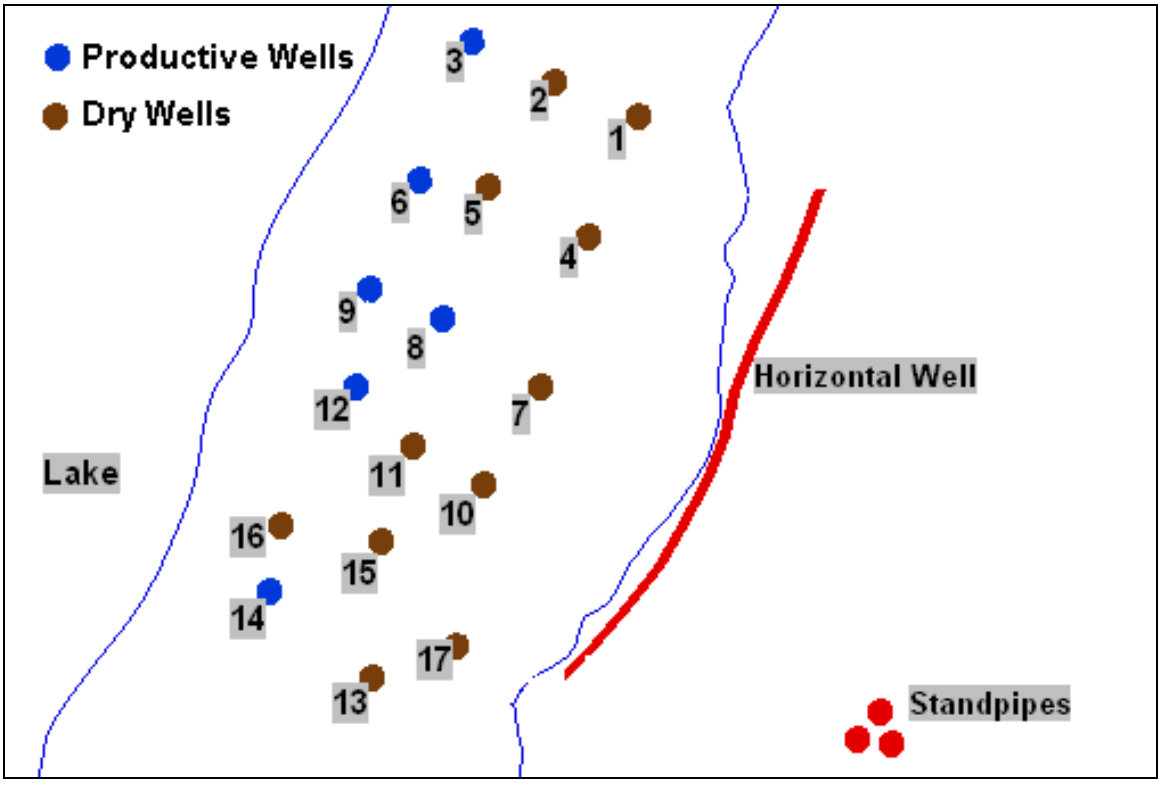


Figure 30. Extraction well locations (blue wells indicate productive pumping wells in May 2004; brown wells were dry in May 2004).

During the individual pumping tests, the flow meters at each well were monitored to determine the rate of extraction as the test progressed. The time and cumulative flow were recorded each time the pump turned on or off. This information was used to calculate the total flow rate by dividing the total volume of water extracted since the beginning of the pump test by the total time. The results are shown for all of the productive wells in Figure 31. Most of the wells had an abnormal start during the first 10 min of the test as the aquifer adjusted to the new extraction. However, all of the plots then flattened off at a flow rate that the aquifer could support.

### Short-term pumping run

The first run with pumping was meant to replicate the last 2 hr of the pumping tests in May 2004. After several tests with only one well on at a time, a final, 2-hr test was run with all of the wells on at once. With so many wells, it was impossible to check the flow rates during the test, but it is assumed that the rates were similar to those measured during the individual tests. The flow values used are shown in Figure 31 and Table 3.

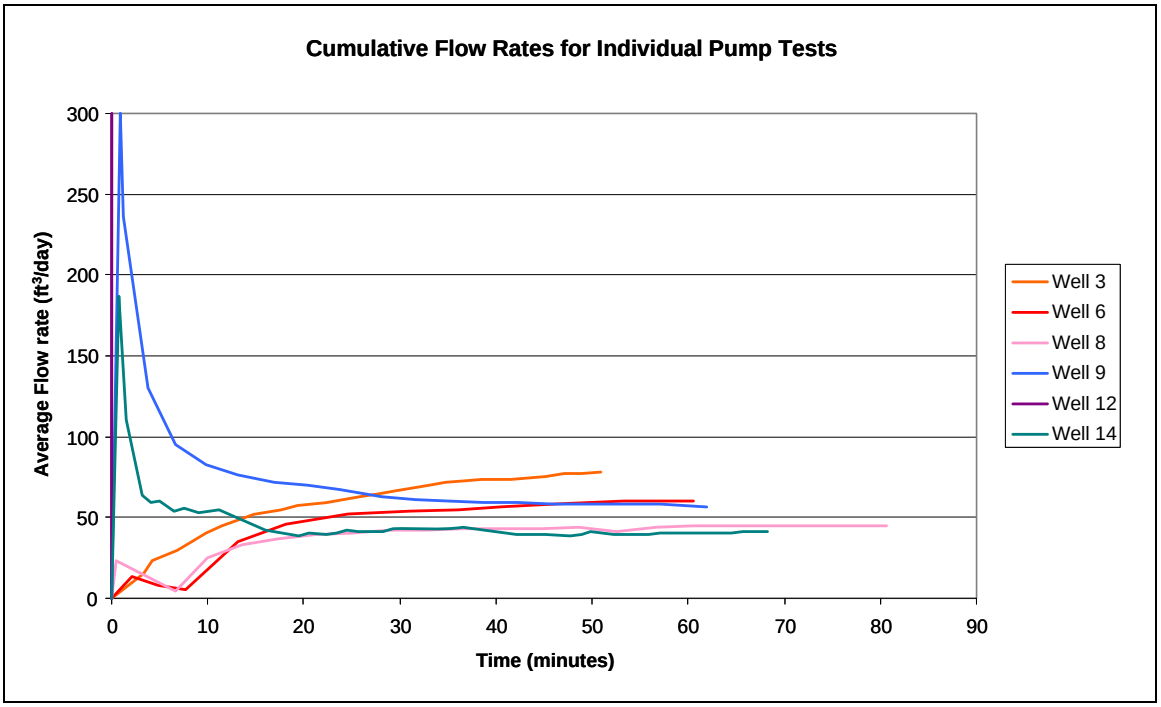


Figure 31. Total flow rates for extraction wells from May 2004 testing.

The piezometers on the bluff face recorded measurements throughout the pumping period. The locations of the piezometers are shown in Figure 32 and Figure 33. Each one was set to a specific depth. Piezometers 8 and 9 actually have two probes set at different depths, making a total of 14 piezometers.

Table 3. Field test flow rate values for productive extraction wells.

| Extraction Well | Flow Rate from Field Testing, $ft^3$/day |
|---|---|
| Well 3 | 78.925 |
| Well 6 | 59.675 |
| Well 8 | 44.275 |
| Well 9 | 57.75 |
| Well 12 | 9.625 |
| Well 14 | 42.35 |

This short-term model was run for 2 hr just like the field test, and the piezometer head values were compared to those measured in the field. The comparisons are shown in the plots in Appendix A.

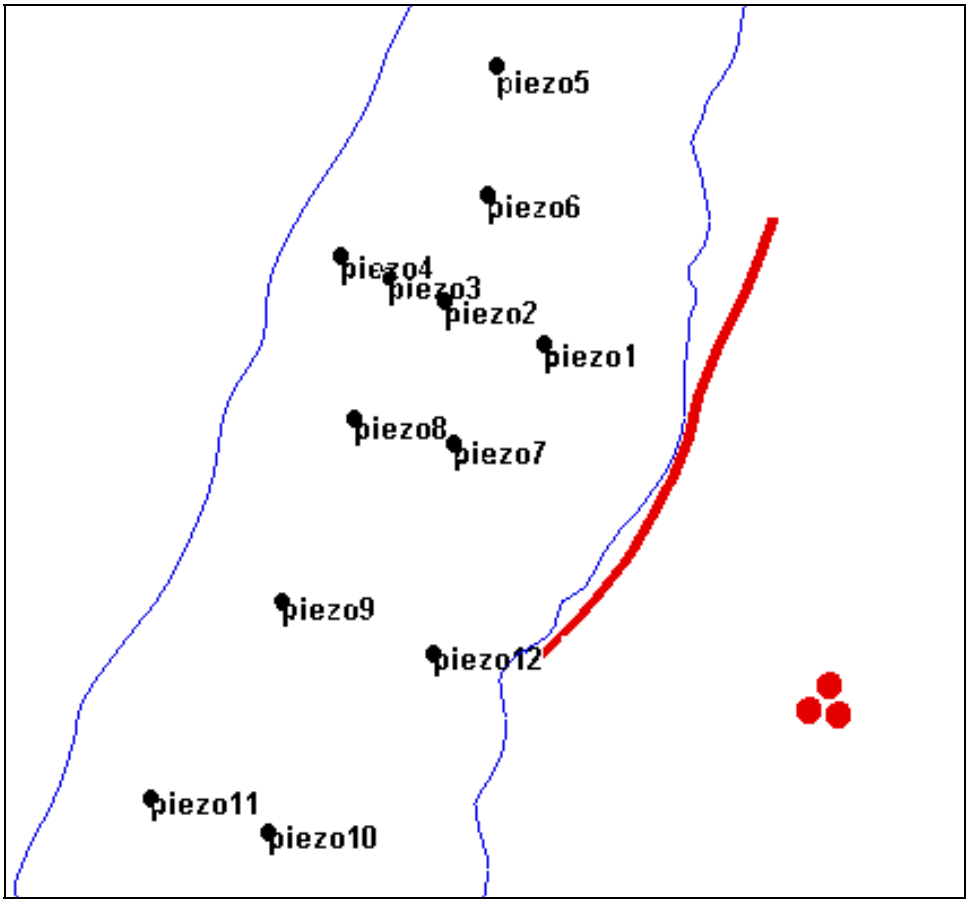


Figure 32. Piezometer locations on bluff face.

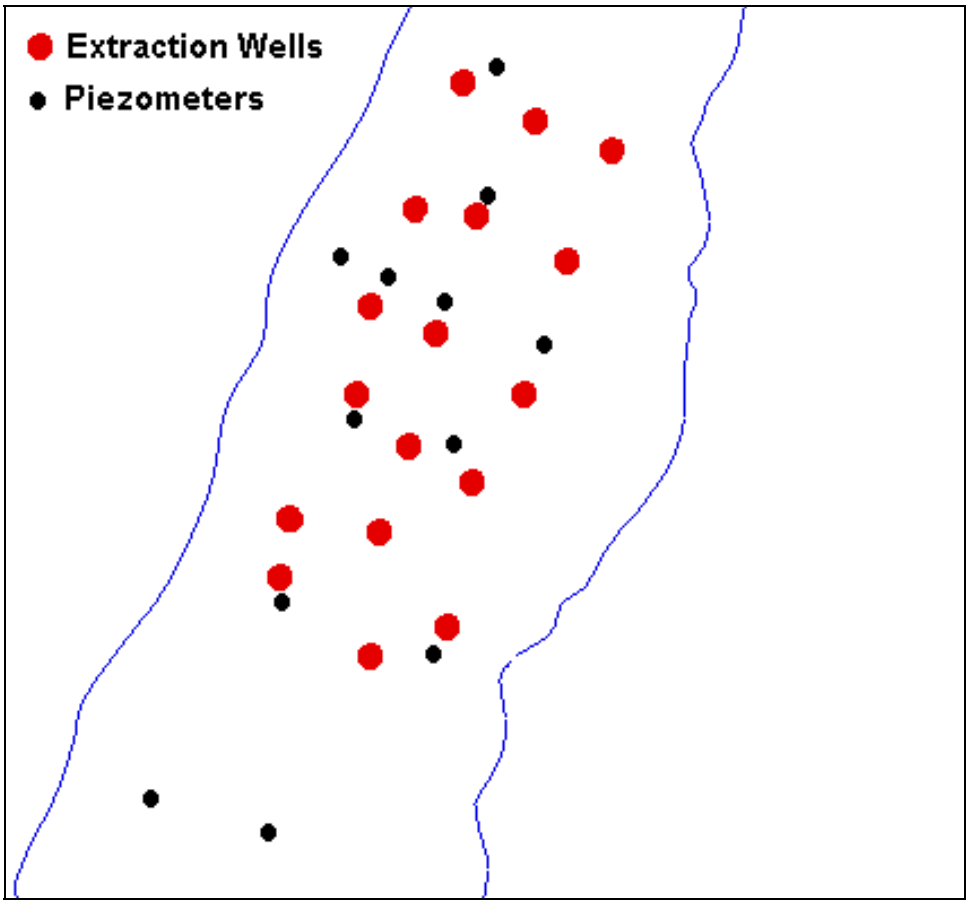


Figure 33. Piezometers and wells on bluff face.

The degree of similarity in the plots is mostly dependent on the correctness of the geology model of the bluff. The connectivity between the well and piezometer locations and the sizes of the sections of conductive materials can cause large differences in the influence of the extraction wells. Although storage and conductivity values have an effect on the pumping results, most of these values have already been calibrated sufficiently using the tests run behind the bluff.

The geology is based mostly on an interpolation of five cross-sectional drawings. This short-term pumping test can reveal how well that interpolation reproduced the actual conditions in the bluff.

In general, the comparison is close. Two piezometers, 2 and 3, had a smaller change in the field than that predicted by the model. Three piezometers, 7, 8(deep), and 9(shallow) had a greater change in the field than that predicted by the model.

### Long-term pumping run

A final run was made to determine the long-term effects of the dewatering scheme on the bluff in these conditions. The tests were run for 100 days, slightly more than 3 months. Initially, the pumping rates were set according to those measured in the field during testing in May 2004. However, in almost all cases, these rates proved to be too high for a long test and the rates were gradually dropped until the well remained wet during the entire period. The rates are listed in Table 4. Only wells 6 and 8 were able to maintain significant extraction rates for the longer period of time.

Table 4. Comparison of field measured extraction rates during 2-hr test and values used in model during 100-day run.

| Extraction Well | Flow Rate from Field Testing ($ft^3$/day) | Flow Rate used in Long-term Pumping Run ($ft^3$/day) |
|---|---|---|
| Well 3 | 78.925 | 0.0 |
| Well 6 | 59.675 | 60.0 |
| Well 8 | 44.275 | 20.0 |
| Well 9 | 57.75 | 0.0 |
| Well 12 | 9.625 | 0.0 |
| Well 14 | 42.35 | 1.0 |

The effects of the pumping on the bluff were smaller than expected. The comparison was made by cutting a cross section passing close to well 6 and well 8, the two most productive wells in the model. The cross-sectional location is shown in Figure 34. The material distribution in Figure 35 shows that both wells are screened in the sand layer directly above the smear zone. Figure 36 shows the degree of saturation on this cross section before the pumping began. The sand layer where the two wells are screened is already dry before pumping begins. Figure 37 shows the same cross section after 100 days of pumping by these two wells. A close comparison shows that the sand layer is slightly dryer, but the difference is not dramatic.

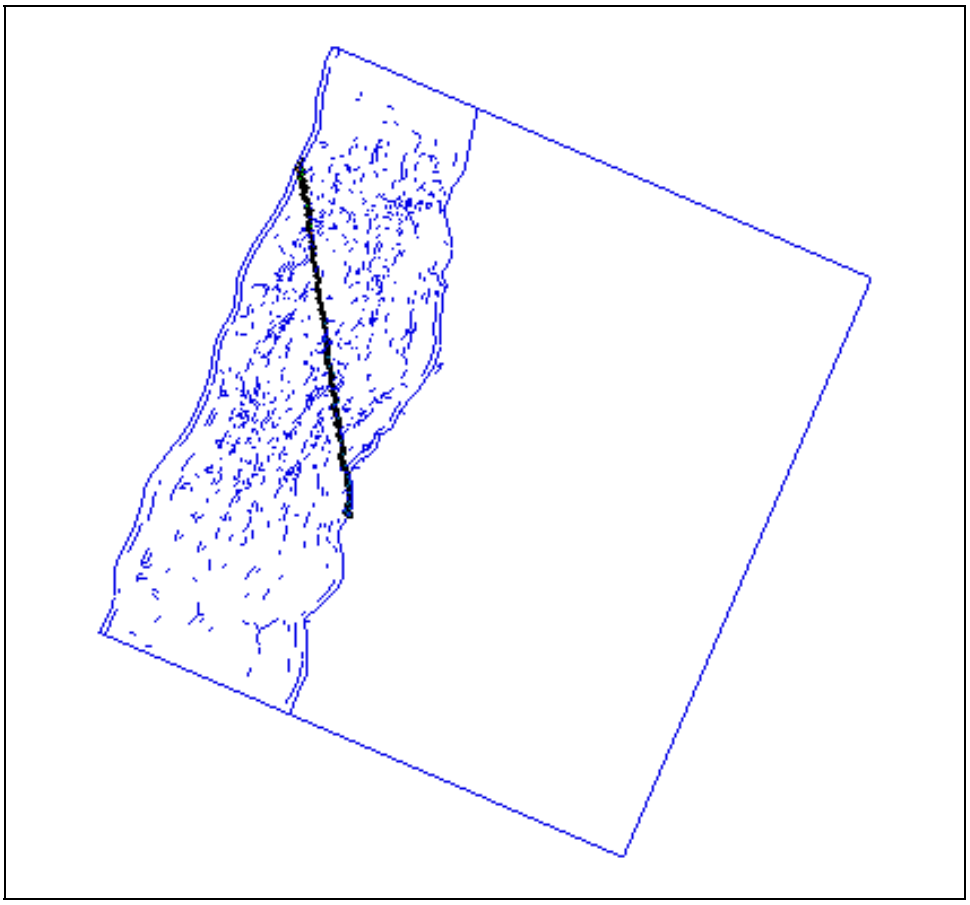

Figure 34. Location of a cross section passing near wells 6 and 8. This cross section is shown on its side in Figure 35 through Figure 37.

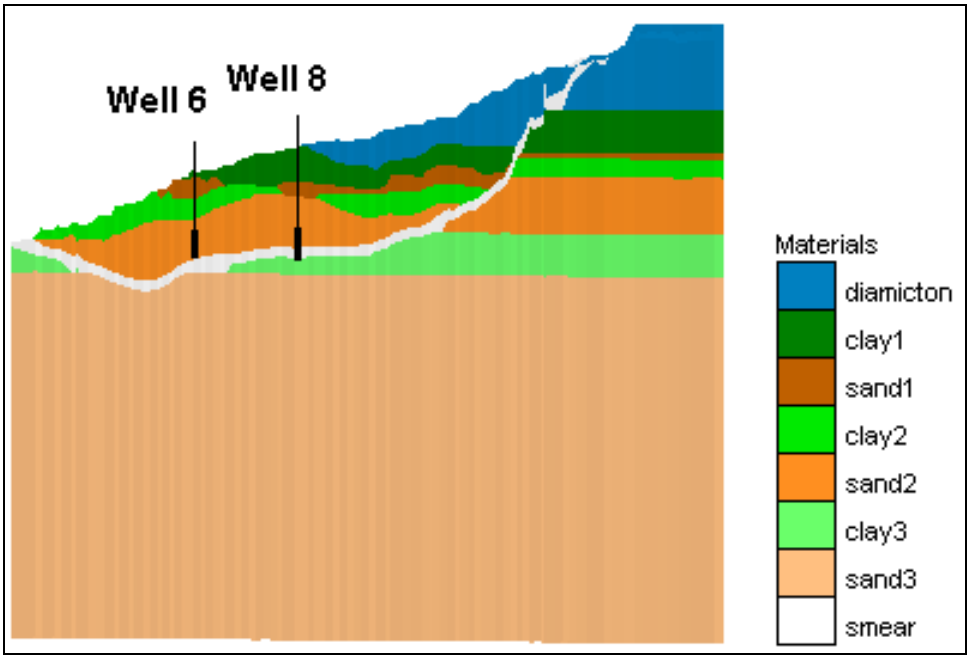


Figure 35. Material distribution on the cross section passing near wells 6 and 8.

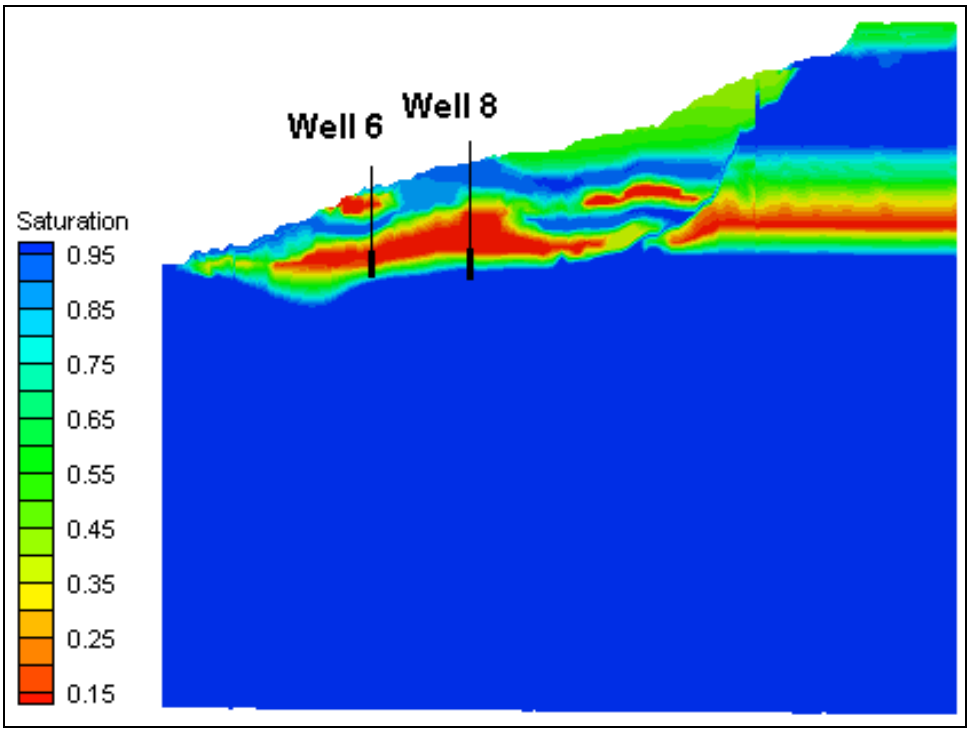


Figure 36. Degree of saturation on a cross section passing near wells 6 and 8 immediately before pumping began (blue areas are completely saturated; red areas are almost completely dry).

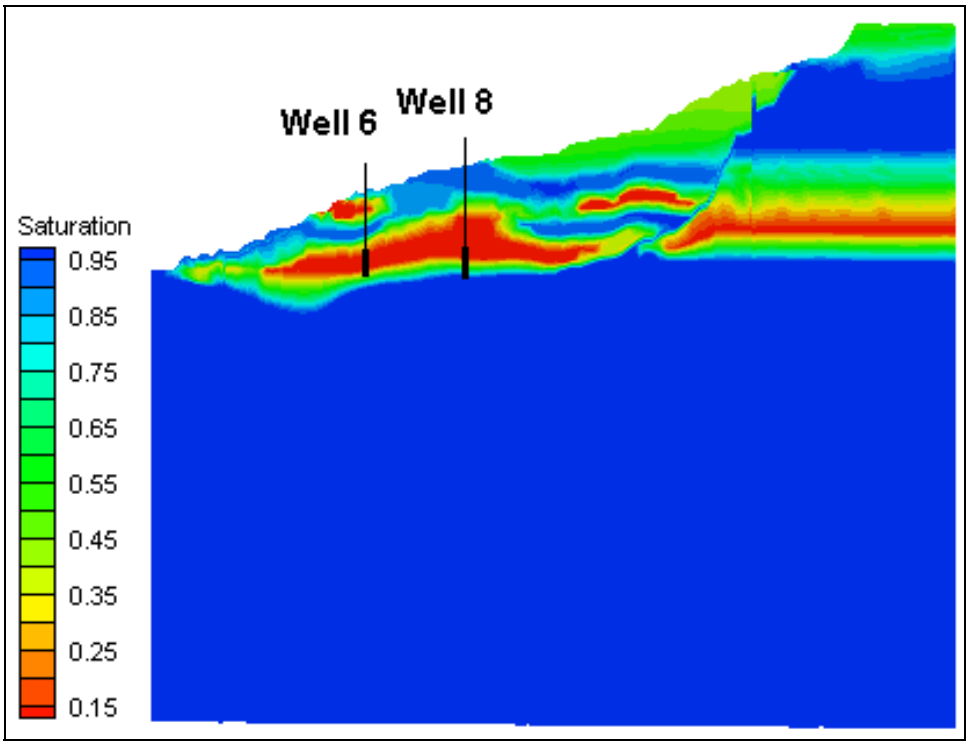


Figure 37. Degree of saturation on a cross section passing near wells 6 and 8 after 100 days of pumping (blue areas are completely saturated; red areas are almost completely dry).

# 9 Conclusions

This model and the analysis had several purposes including the showcasing of the application of groundwater modeling techniques to a coastal preservation project involving complicated geology and the analysis of the possible effectiveness of the dewatering scheme.

## Quality of model

The replication of the geology of the site is good, in general, because of the large amount of data. However, there were some disappointing differences in the piezometer responses to extraction wells and in the available water for each of the extraction wells, showing that the interpolation areas between the data locations may not be as well modeled.

The calibration of this model is good compared to other groundwater models in general usage. The model replicated most of the tests in the standpipes behind the bluff face exceptionally well. The parameter values derived from the calibration process can be accepted confidently.

The simulation of the pumping is as good as the geology and the calibration in general. However, because the calibration was made to May 2004 data and the pumping was continued with those same boundary conditions, many of the extraction wells were dry and there was not much water to be removed. The pumping simulations could be much more informative and useful if they were performed on a model run during a wetter period of time.

Also disappointing was the lack of water available to many of the wells, which were productive during the field testing. It is possible that the smear zone was holding too much water back, resulting in a drier bluff area than that existing at the site. More testing and site measurements would be needed to address this concern.

## Analysis of dewatering system

The analysis of the dewatering system is difficult because the model was already so dry, but it appears that the extraction wells did not have a large zone of influence. Even 100 days of pumping in two productive wells barely had a visible effect on the saturation of the soil nearby. It seems

unlikely that the wells spaced so far apart could sufficiently dewater the bluff face to prevent annual spring bluff failures.

The horizontal well obviously dewaters the area nearby and works exactly as one would expect. The problem with this well is that its influence does not seem to affect the saturation on the bluff face. This is probably due to the smear zone, which separates the bluff system from that behind the bluff face. Secondly, the horizontal well's influence does not extend very deep – not even to the bottom of the diamicton layer.

In February 2006, Dr. Ron Chase made an informal presentation showing the effects of dewatering on the first season. His data also showed the effects the dewatering seemed to have on the bluff stability. Preliminary results seem to show that while the dewatering scheme does not completely stop bluff movement, it does slow it considerably. More study is necessary to confirm this conclusion and to determine how it relates to the effects seen in the model.

From the analysis of the model, it seems that a good solution would be to dewater the bluff using extraction wells placed back behind the bluff face, perhaps near the location of the standpipes used for slug testing. In this way, the wells could stop flow from entering the bluff area from several different depths and layers. Instead of removing water that has already entered the highly complicated geology on the bluff face, the water could be removed before it arrives. In this area, a few wells could pump at higher rates and improve the efficiency of the system.

## Suggestions for future study

Greater knowledge can be gained concerning the accuracy of the geology and the quality of the dewatering system by running the model in a wetter season. The required data may already exist from previous years of observations at the site. The changes to the model would be an increase in the upstream boundary conditions, determined from standpipe head measurements during wetter seasons, and perhaps an increase in the rainfall applied to the top of the model. In addition, an extra set of field tests from a different season could be used to fine-tune the calibration. The original tests from May 2004 were generally not run long enough to gather sufficient information and did not include many of the wells which were dry at the time.

Original plans were to reprogram ADH to handle wells that turn on and off based on the groundwater head. Time constraints resulted in other simplifications to achieve a similar effect, but the added capability could still be useful – especially if a longer simulation were to be run with seasonal changes.

Much has already been mentioned about the tools to interpolate the geology and convert it to a numerical mesh. These tools will continue to evolve to be more and more useful. When they have improved, this model should be rebuilt with a smoother mesh and, therefore, faster run-times.

Because the interpolation issues have caused difficulties with the geologic model, it would be useful to use a geostatistics model, such as T-PROGS to simulate several possibilities for the geology and compare the outcomes for each model. This type of analysis would be especially useful in a model like this because of the high variablility of the material distributions and the fact that interpolation cannot always reproduce actual conditions accurately.

# References

Chase, R. B., K. E. Chase, A. E. Kehew, and W. W. Montgomery. 2001a. Determining the kinematics of slope movements using low-cost monitoring and cross-section balancing. *Environmental and Engineering Geoscience* VII(2): 193-203.

Chase, R. B., A. E. Kehew, and W. W. Montgomery. 2001b. Significance of ground water in triggering cohesive bluff failures, Lake Michigan case study. In *Proceedings of the Coastal Zone 01 Conference, NOAA*, Cleveland, OH.

Lemon, A. L., and N. L. Jones 2003a. Building solid models from boreholes and user-defined cross-sections. *Computers and Geosciences* 29(5): 547-555.

Lemon, A. L, N. L. Jones, and J. E. Greer. 2003b. A horizons-based approach to modeling complex geology. In *MODFLOW and More 2003: Understanding through Modeling – Conference Proceedings*, September 16-19, Colorado School of Mines, 666-670.

Schmidt, J. H. 1995. A 3-D adaptive finite element method for transport processes. MS thesis, University of Texas at Austin.

Howington, S. E., R. C. Berger, J. P. Hallberg, J. F. Peters, A. K. Stagg, E. W. Jenkins, and C. T. Kelley. 1999. A model to simulate the interaction between groundwater and surface water. In *Proceedings of the 1999 High-Performance Computing Users' Group Meeting, Monterey, CA, USA*. Washington, DC: DoD HPC Modernization Office.

# Appendix A: Model Prediction and Field Measurement Comparisons

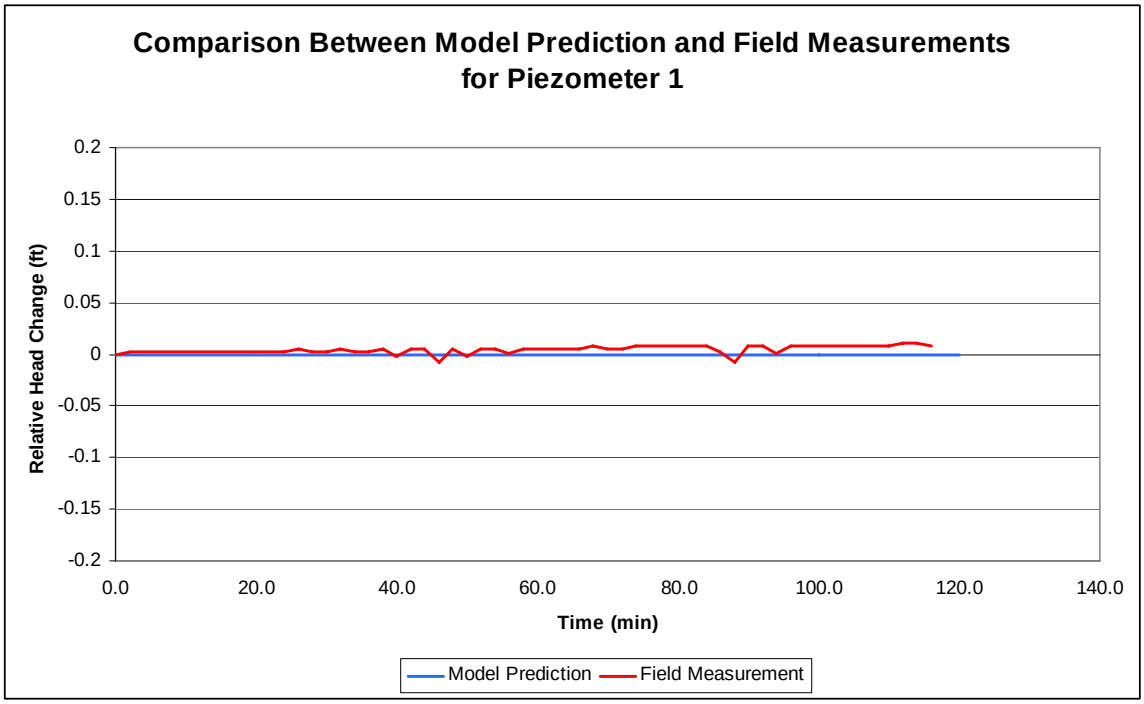

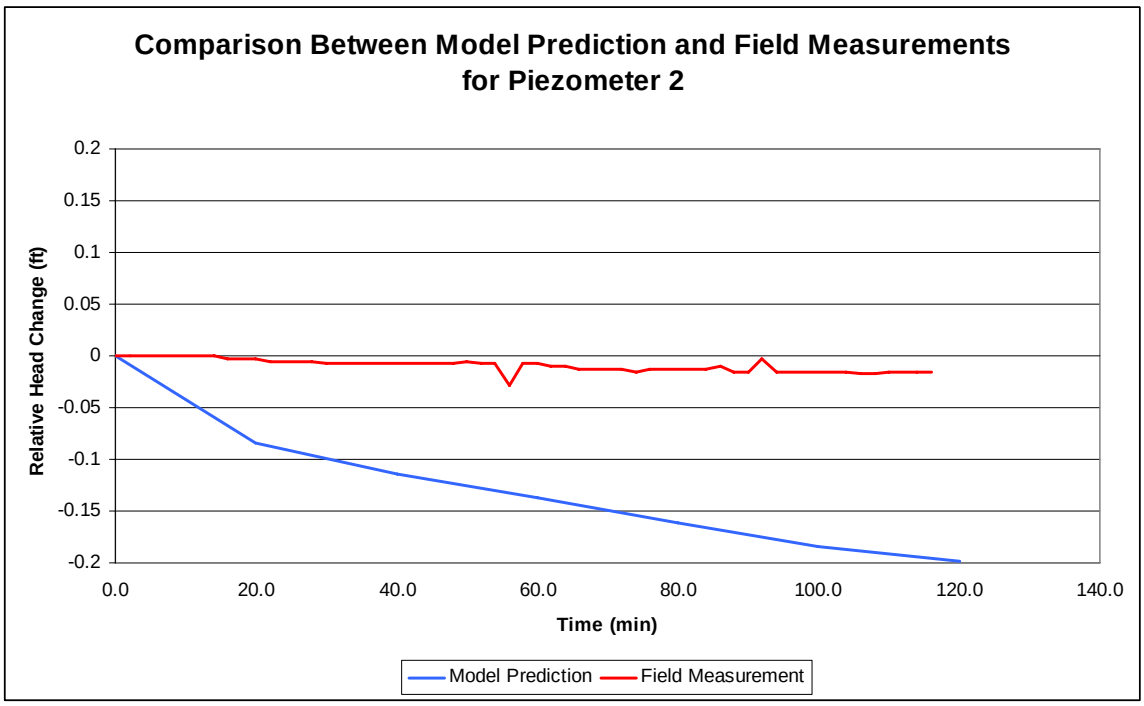
Comparison Between Model Prediction and Field Measurements for Piezometer 2
Relative Head Change (ft)
0.2
0.15
0.1
0.05
0
-0.05
-0.1
-0.15
-0.2
0.0
20.0
40.0
60.0
80.0
100.0
120.0
140.0
Time (min)
Model Prediction
Field Measurement

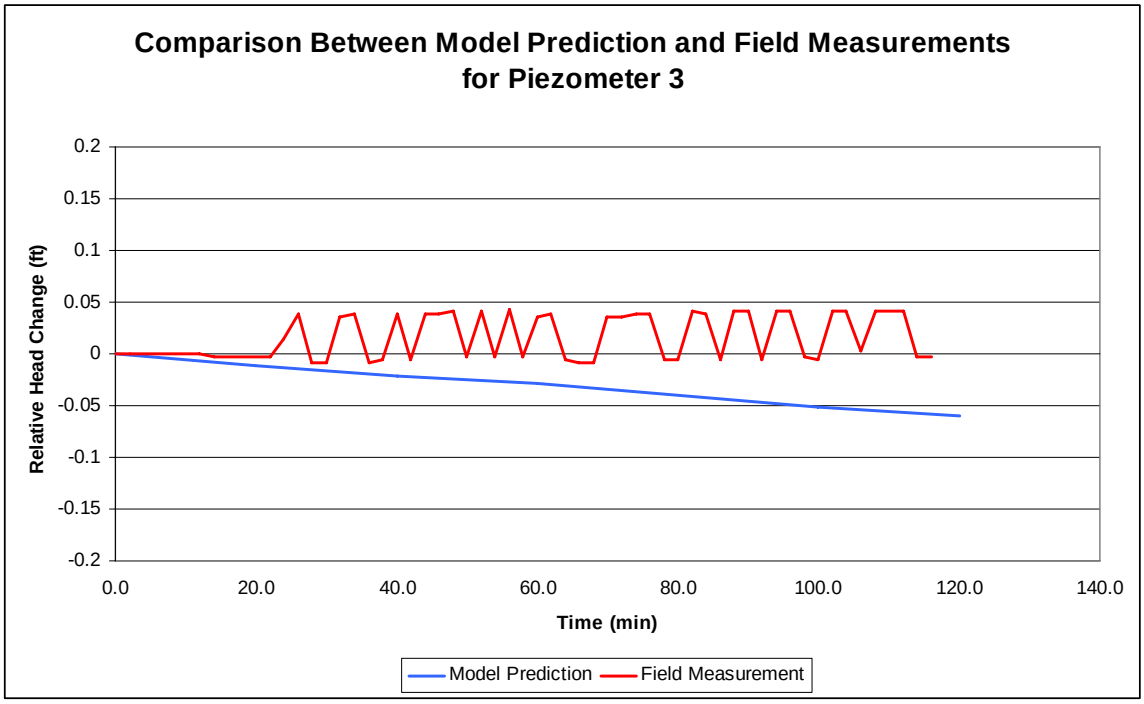
Comparison Between Model Prediction and Field Measurements for Piezometer 3
Relative Head Change (ft)
0.2
0.15
0.1
0.05
0
-0.05
-0.1
-0.15
-0.2
0.0
20.0
40.0
60.0
80.0
100.0
120.0
140.0
Time (min)
Model Prediction
Field Measurement

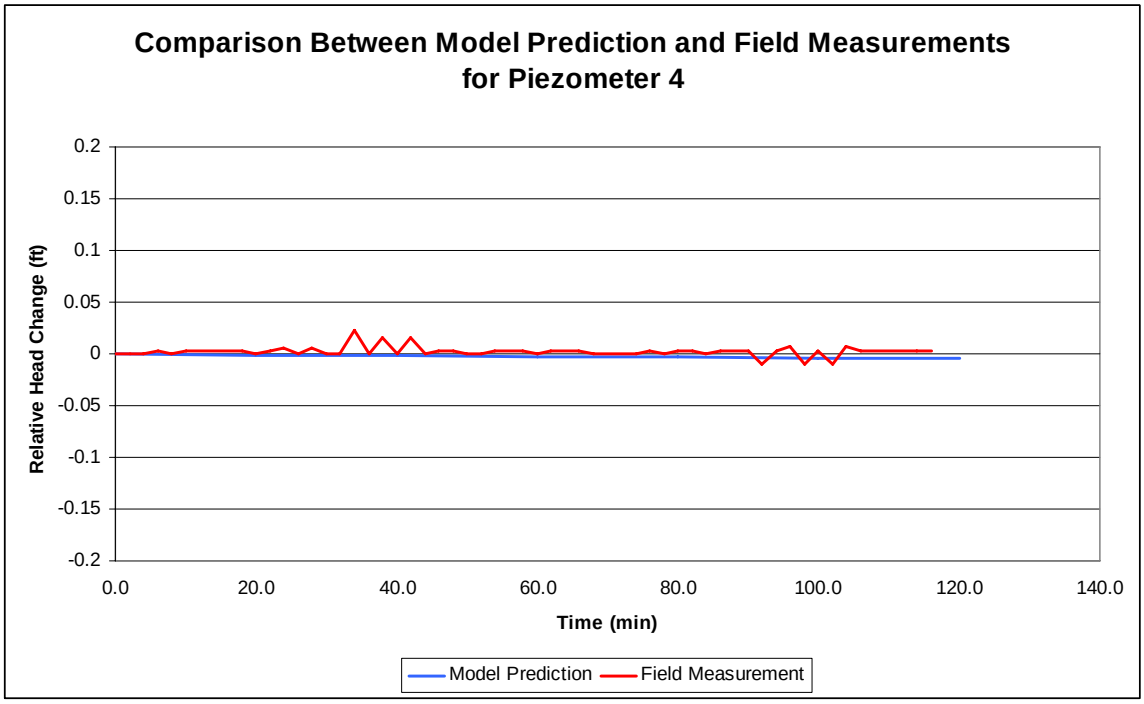
Comparison Between Model Prediction and Field Measurements for Piezometer 4
Relative Head Change (ft)
0.2
0.15
0.1
0.05
0
-0.05
-0.1
-0.15
-0.2
0.0
20.0
40.0
60.0
80.0
100.0
120.0
140.0
Time (min)
Model Prediction
Field Measurement

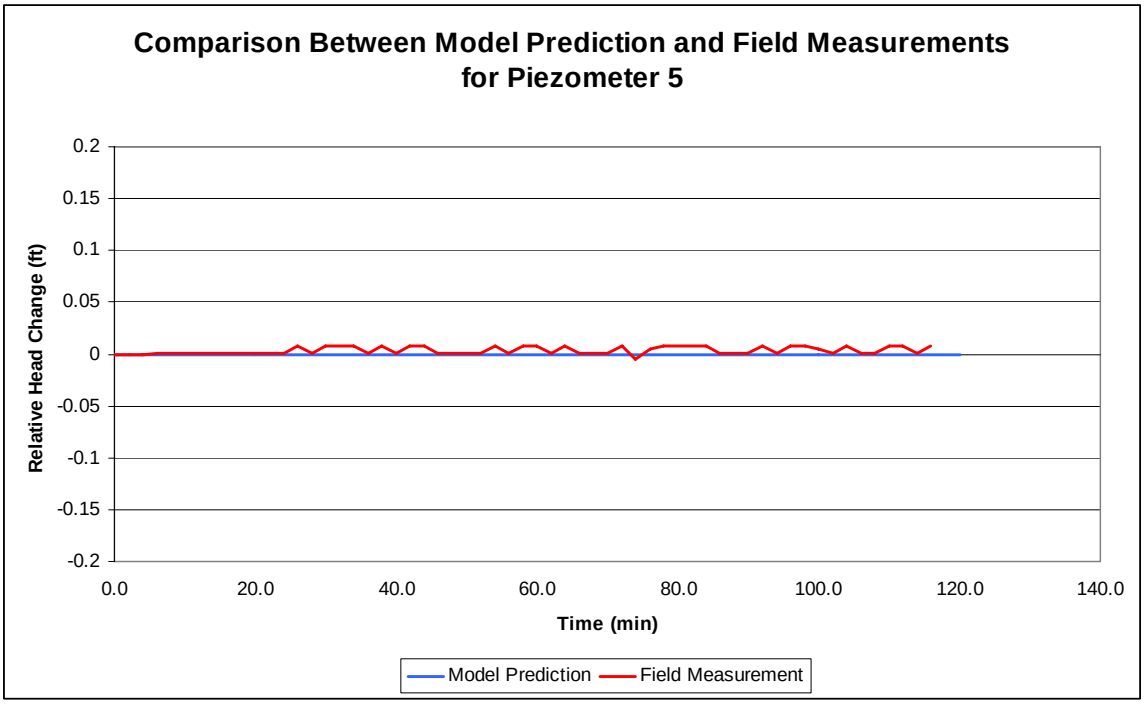
Comparison Between Model Prediction and Field Measurements for Piezometer 5
Relative Head Change (ft)
0.2
0.15
0.1
0.05
0
-0.05
-0.1
-0.15
-0.2
0.0
20.0
40.0
60.0
80.0
100.0
120.0
140.0
Time (min)
Model Prediction
Field Measurement

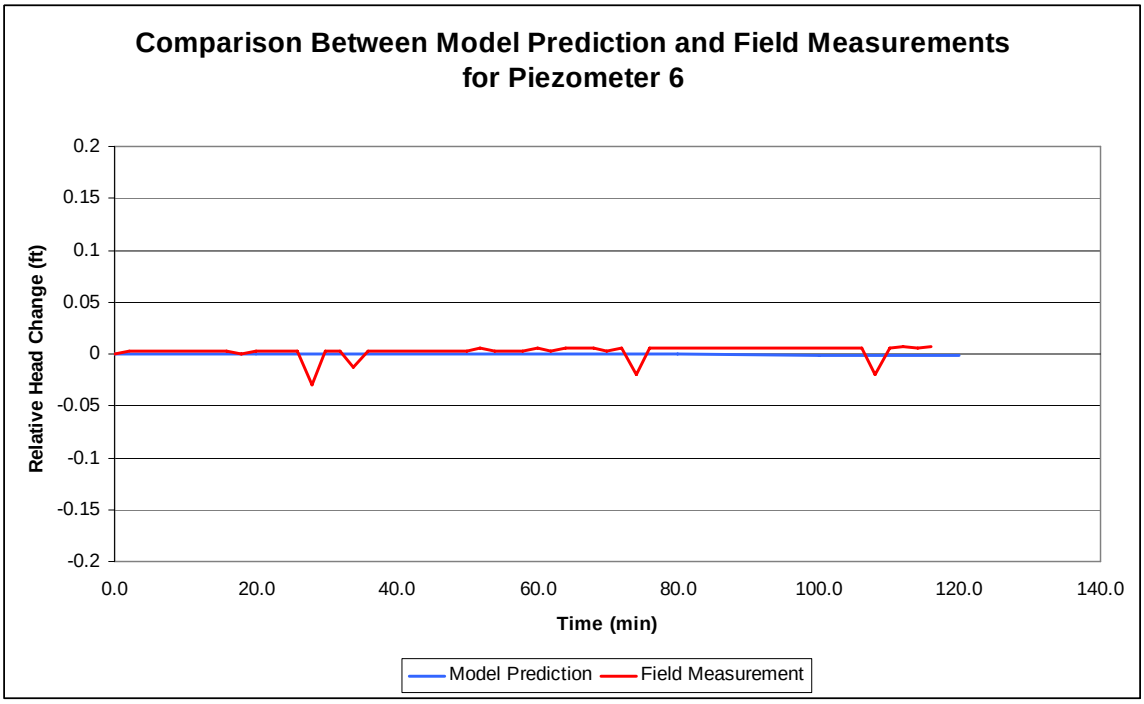
Comparison Between Model Prediction and Field Measurements for Piezometer 6
Relative Head Change (ft)
0.2
0.15
0.1
0.05
0
-0.05
-0.1
-0.15
-0.2
0.0
20.0
40.0
60.0
80.0
100.0
120.0
140.0
Time (min)
Model Prediction
Field Measurement

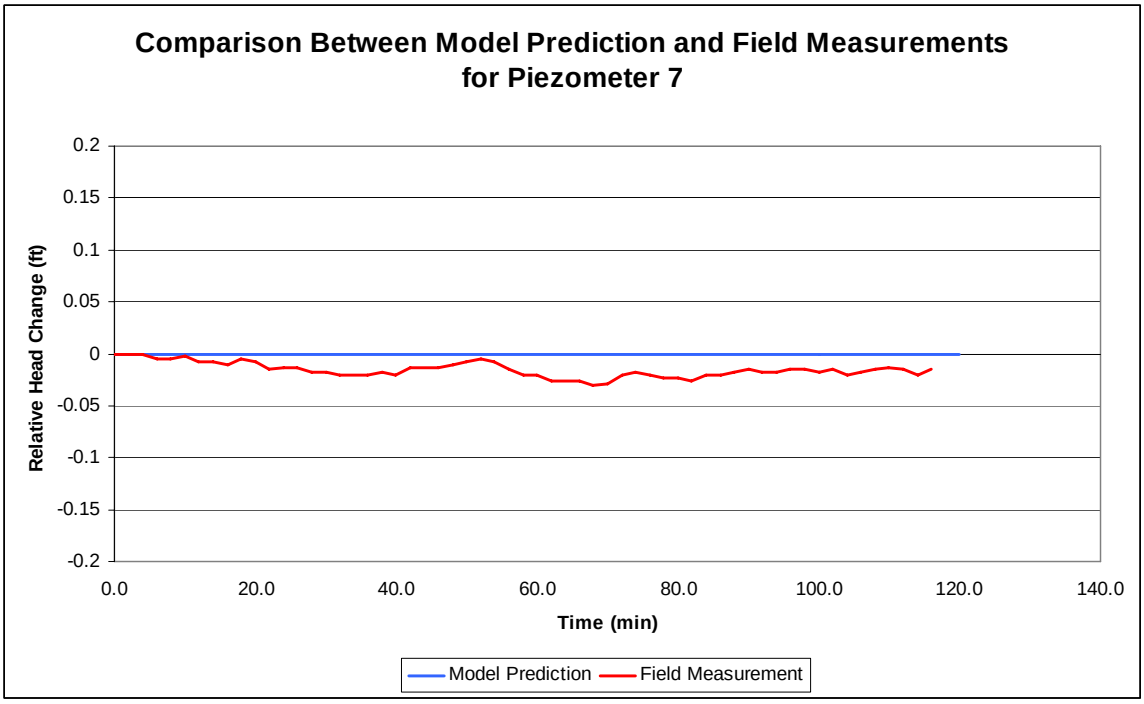
Comparison Between Model Prediction and Field Measurements for Piezometer 7
Relative Head Change (ft)
0.2
0.15
0.1
0.05
0
-0.05
-0.1
-0.15
-0.2
0.0
20.0
40.0
60.0
80.0
100.0
120.0
140.0
Time (min)
Model Prediction
Field Measurement

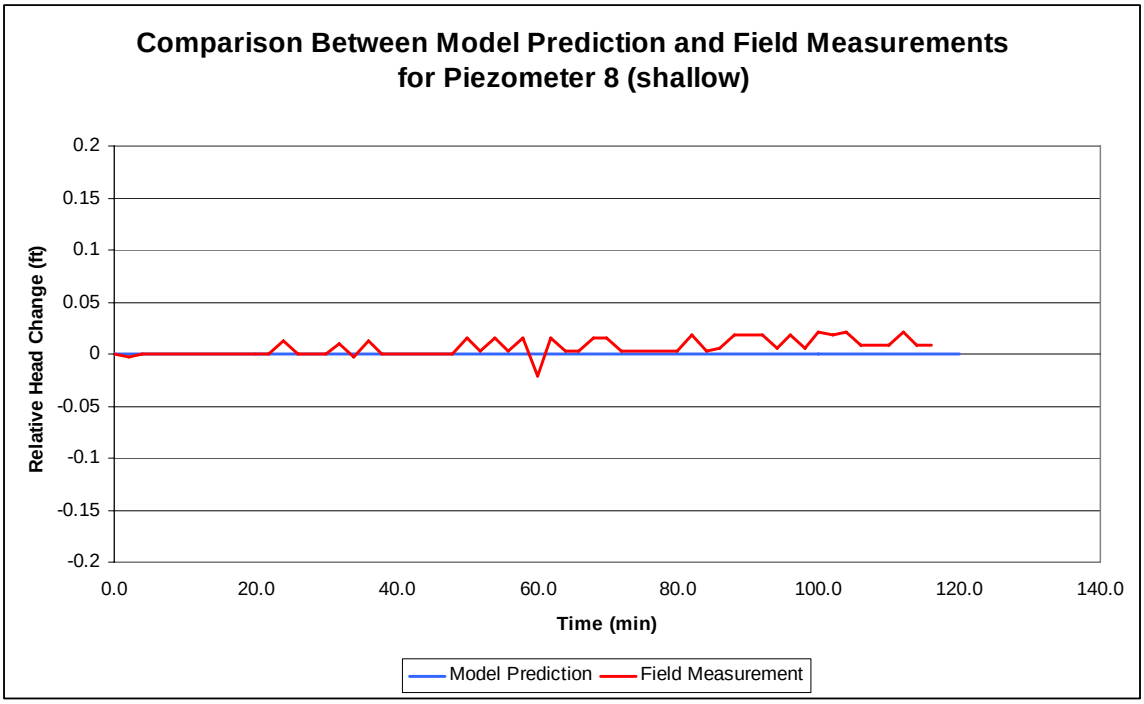
Comparison Between Model Prediction and Field Measurements for Piezometer 8 (shallow)
Relative Head Change (ft)
0.2
0.15
0.1
0.05
0
-0.05
-0.1
-0.15
-0.2
0.0
20.0
40.0
60.0
80.0
100.0
120.0
140.0
Time (min)
Model Prediction
Field Measurement

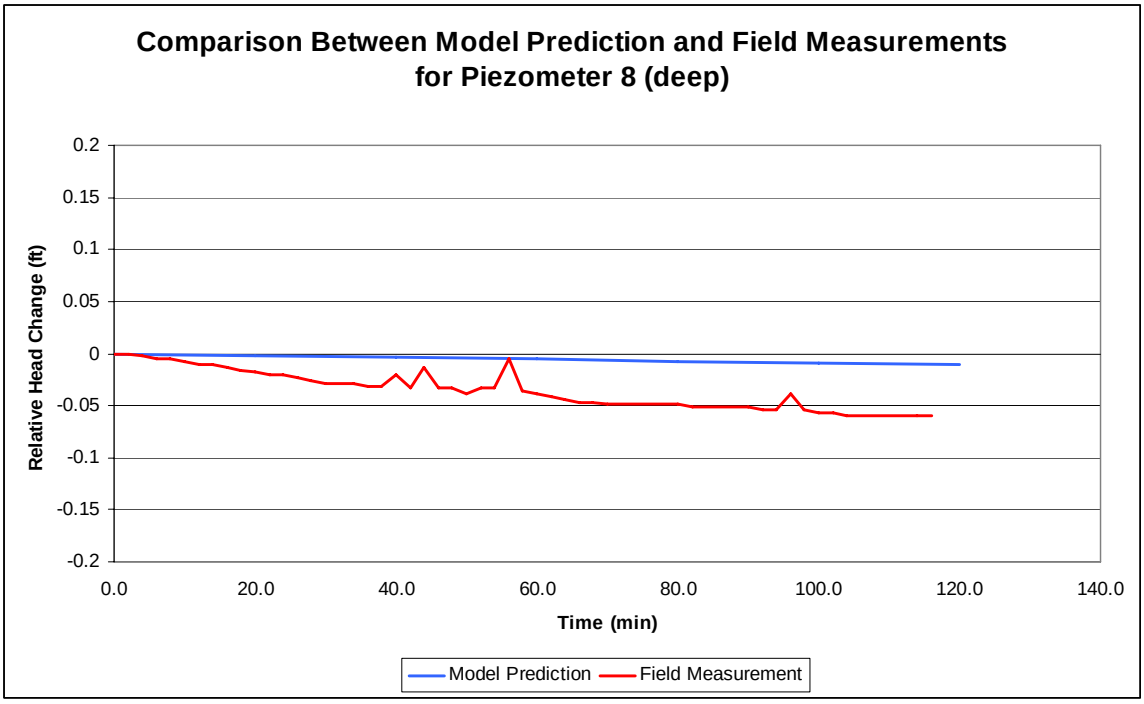
Comparison Between Model Prediction and Field Measurements for Piezometer 8 (deep)
Relative Head Change (ft)
0.2
0.15
0.1
0.05
0
-0.05
-0.1
-0.15
-0.2
0.0
20.0
40.0
60.0
80.0
100.0
120.0
140.0
Time (min)
Model Prediction
Field Measurement

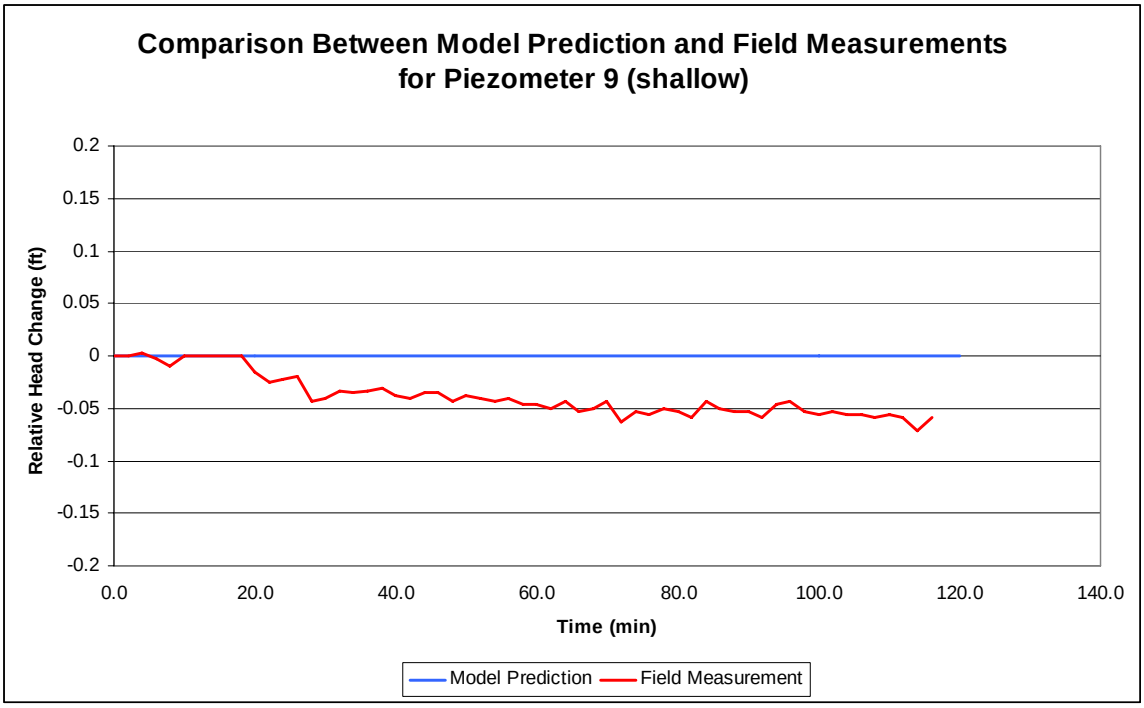
Comparison Between Model Prediction and Field Measurements for Piezometer 9 (shallow)
Relative Head Change (ft)
0.2
0.15
0.1
0.05
0
-0.05
-0.1
-0.15
-0.2
0.0
20.0
40.0
60.0
80.0
100.0
120.0
140.0
Time (min)
Model Prediction
Field Measurement

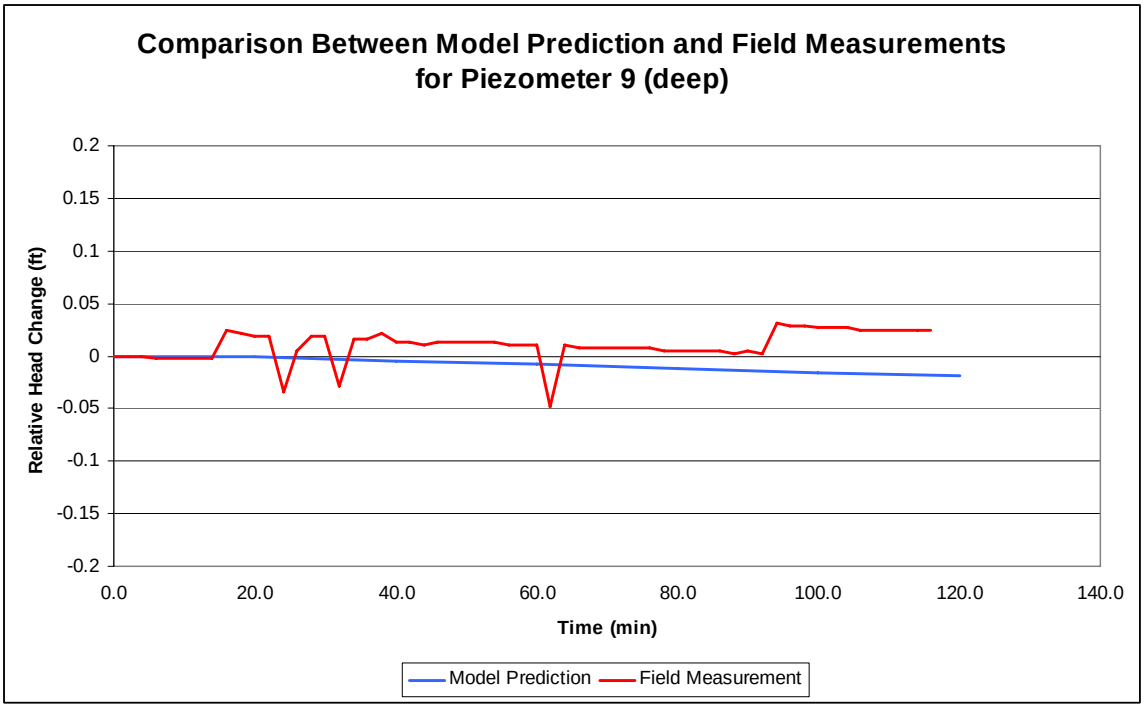
Comparison Between Model Prediction and Field Measurements for Piezometer 9 (deep)
Relative Head Change (ft)
0.2
0.15
0.1
0.05
0
-0.05
-0.1
-0.15
-0.2
0.0
20.0
40.0
60.0
80.0
100.0
120.0
140.0
Time (min)
Model Prediction
Field Measurement

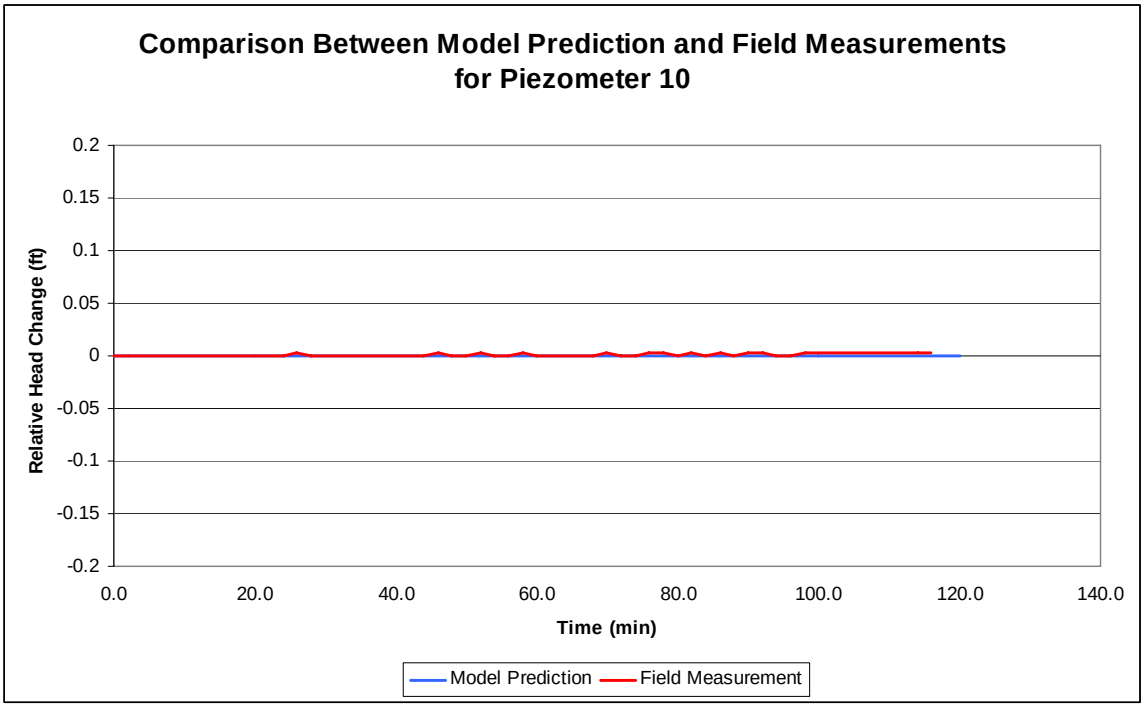
Comparison Between Model Prediction and Field Measurements for Piezometer 10
Relative Head Change (ft)
0.2
0.15
0.1
0.05
0
-0.05
-0.1
-0.15
-0.2
0.0
20.0
40.0
60.0
80.0
100.0
120.0
140.0
Time (min)
Model Prediction
Field Measurement

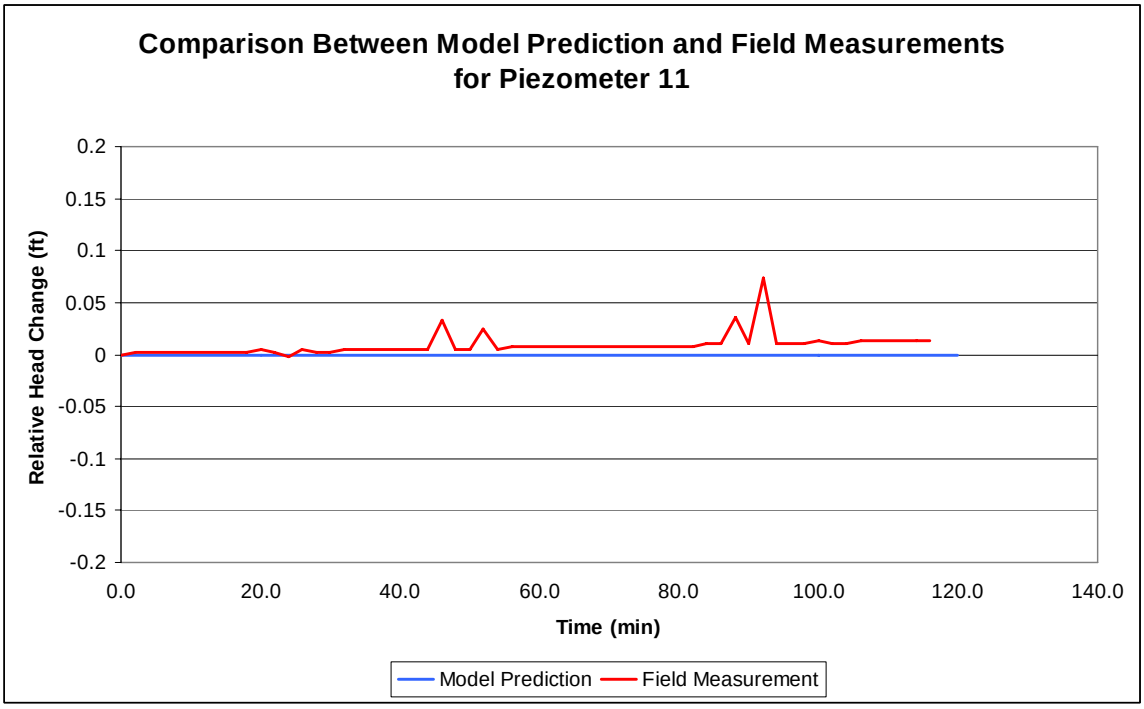
Comparison Between Model Prediction and Field Measurements for Piezometer 11
Relative Head Change (ft)
0.2
0.15
0.1
0.05
0
-0.05
-0.1
-0.15
-0.2
0.0
20.0
40.0
60.0
80.0
100.0
120.0
140.0
Time (min)
Model Prediction
Field Measurement

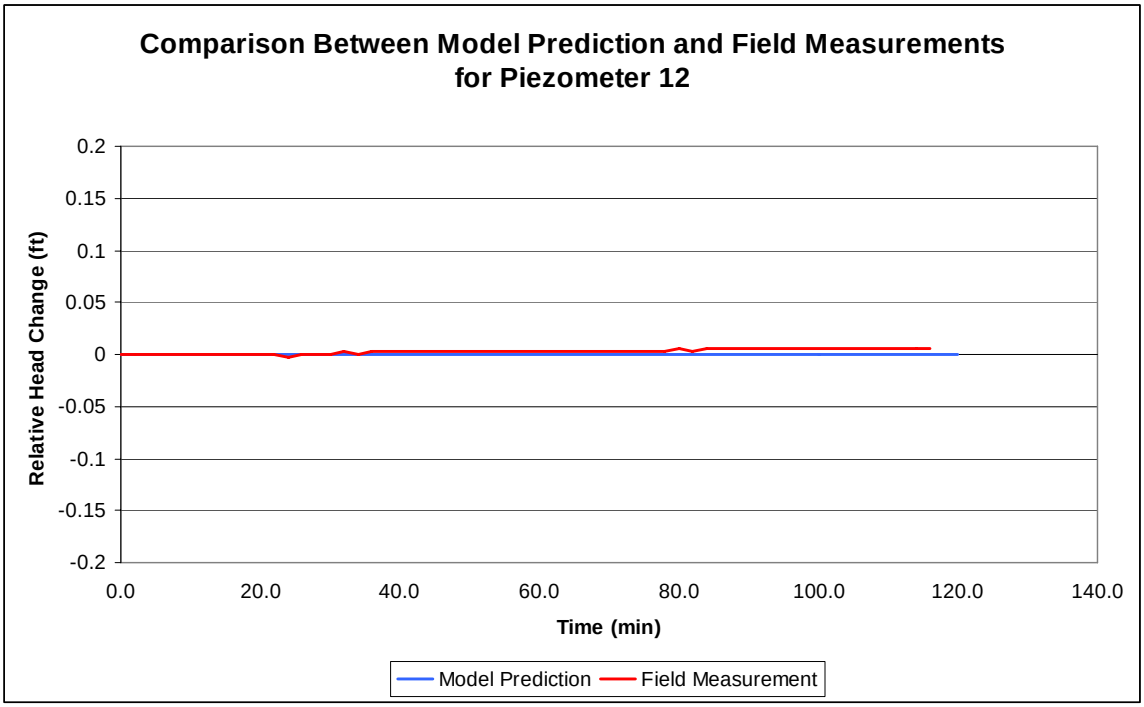
Comparison Between Model Prediction and Field Measurements for Piezometer 12
Relative Head Change (ft)
0.2
0.15
0.1
0.05
0
-0.05
-0.1
-0.15
-0.2
0.0
20.0
40.0
60.0
80.0
100.0
120.0
140.0
Time (min)
Model Prediction
Field Measurement

# REPORT DOCUMENTATION PAGE

*Form Approved*
*OMB No. 0704-0188*



| 1. REPORT DATE *(DD-MM-YYYY)* | 2. REPORT TYPE | 3. DATES COVERED *(From - To)* |
|---|---|---|
| September 2007 | Final report | |

**4. TITLE AND SUBTITLE**

Flow Model Study for Section 227 Demonstration Project in Allegan County, Michigan

**5a. CONTRACT NUMBER**

**5b. GRANT NUMBER**

**5c. PROGRAM ELEMENT NUMBER**

**6. AUTHOR(S)**

Clarissa P. Hansen, Stacy E. Howington, and M. Eileen Glynn

**5d. PROJECT NUMBER**

**5e. TASK NUMBER**

**5f. WORK UNIT NUMBER**

**7. PERFORMING ORGANIZATION NAME(S) AND ADDRESS(ES)**

See reverse.

**8. PERFORMING ORGANIZATION REPORT NUMBER**

ERDC TR-07-12

**9. SPONSORING / MONITORING AGENCY NAME(S) AND ADDRESS(ES)**

U.S. Army Corps of Engineers
Washington, DC 20314-1000

**10. SPONSOR/MONITOR'S ACRONYM(S)**

**11. SPONSOR/MONITOR'S REPORT NUMBER(S)**

**12. DISTRIBUTION / AVAILABILITY STATEMENT**

Approved for public release; distribution is unlimited.

**13. SUPPLEMENTARY NOTES**

**14. ABSTRACT**

The National Shoreline Erosion Control Development and Demonstration Program (Section 227) is authorized by Congress under Section 227 of the Water Resources and Development Act of 1996. The program provided funding to research projects for the development and evaluation of innovative methods of shoreline erosion abatement. This report describes a numerical flow model developed for the Allegan County Bluff Stabilization Project within the Section 227 Demonstration Program. The Bluff Stabilization Site is located just north of Southaven, MI, and lies on the east coast of Lake Michigan.

Bluff recession and subsequent property loss from bluff erosion is a perpetual process along the coastlines of the Great Lakes. Historically, engineers have protected the toe of the bluff from erosion with seawalls, revetments, dikes, etc., to slow bluff recession. For many bluffs, toe protection helps little because the bluff (slope) frequently fails above the protected toe, at elevations affected by perched water tables exiting at the bluff face.

(Continued)

**15. SUBJECT TERMS**

ADdaptive Hydrology/Hydraulics (ADH)
Bluff dewatering
Bluff recession
Groundwater Modeling System
Lake Michigan
Numerical modeling
Slope stability modeling

| 16. SECURITY CLASSIFICATION OF: | | | 17. LIMITATION OF ABSTRACT | 18. NUMBER OF PAGES | 19a. NAME OF RESPONSIBLE PERSON |
|---|---|---|---|---|---|
| a. REPORT | b. ABSTRACT | c. THIS PAGE | | | 19b. TELEPHONE NUMBER *(include area code)* |
| UNCLASSIFIED | UNCLASSIFIED | UNCLASSIFIED | | 60 | |

**7. (Concluded)**

Malcolm Pirnie, Inc.
640 Freedom Business Center
King of Prussia, PA 19406;
U.S. Army Engineer Research and Development Center
Coastal and Hydraulics Laboratory and Geotechnical and Structures Laboratory
3909 Halls Ferry Road, Vicksburg, MS 39180-6199

**14. (Concluded)**

The Bluff Stabilization Project has focused on the study and control of the groundwater within the bluffs and measurement of its effect on slope stability. The project has spanned over 11 years, led by Dr. Ronald Chase at Western Michigan University, Kalamazoo, MI. The many years of data exhibit a positive correlation between slope movement, freezing ambient air temperatures, and increased soil pore pressures. Thus, decreasing the pore pressures during freezing temperatures may reduce bluff recession.

A dewatering program was started in 2005 to test this hypothesis. This report describes the development of a numerical model of groundwater flow for the purpose of optimizing pumping at the test site. The flow model was constructed using the Groundwater Modeling System (GMS) with the computational code, ADaptive Hydrology/Hydraulics (ADH).